

**INVESTIGATION OF LEAD-FREE BISMUTH PEROVSKITE BY NUMERICAL
SIMULATION USING SCAPS.**

**A THESIS PRESENTED TO THE DEPARTMENT OF MATERIAL SCIENCE AND
ENGINEERING**

AFRICAN UNIVERSITY OF SCIENCE AND TECHNOLOGY, ABUJA



**IN PARTIAL FULFILMENT OF THE REQUIREMENTS FOR THE DEGREE OF
MASTER OF SCIENCE**

BY

OBI, UCHENNA CHARLES

ABUJA, NIGERIA

JULY, 2019

CERTIFICATION

This is to certify that the thesis titled “investigation of lead-free bismuth perovskite by numerical simulation using SCAPS” submitted to the school of postgraduate studies, African University of Science and Technology (AUST), Abuja, Nigeria for the award of the Master's degree is a record of original research carried out by OBI UCHENNA CHARLES in the Department of Material Science and Engineering.

**INVESTIGATION OF LEAD-FREE BISMUTH PEROVSKITE BY NUMERICAL
SIMULATION USING SCAPS**

By

OBI, UCHENNA CHARLES

A THESIS APPROVED BY THE MATERIAL SCIENCE AND ENGINEERING
DEPARTMENT

RECOMMENDED:

.....

Supervisor, Dr. Abdulhakeem Bello

.....

Professor Azikiwe Peter Onwualu

Head, Department of Material Science and Engineering

APPROVED:

.....

Professor Charles Chidume

Chief Academic Officer

.....

June, 2019

ABSTRACT

The theoretical study of methylammonium bismuth halide, $(\text{CH}_3\text{NH}_3)_3\text{Bi}_2\text{I}_9$, was simulated using SCAPS 1D software package. The effect of the bismuth perovskite absorber layer thickness on the solar cell performance was investigated using three different materials (organic and inorganic) materials such as Cu_2O , CuI , and spiro-OMeTAD as hole transporting layer (HTL), and four different materials (organic and inorganic) materials such as ZnO , TiO_2 , PCBM, and P_3HT as electron transporting layer (ETL). The performance of the cell largely depends on the thickness of the absorbing layer, and on the type and combination of ETL and HTL used. The device with Cu_2O as the HTL and ZnO as the ETL showed the best performance at an absorber thickness of 200 nm. The effect of temperature was carried out on the various cell structure, which exhibited different responses to increasing temperature, showing again that the dependence of the solar cell characteristics on the transport layers. Generally, there was a change in the performance of the solar cell devices as the temperature changes. Results obtained from this work showed that to get the optimum cell performance at a low cost, the device should be fabricated with inorganic transport materials, this will help in solving the issue of poor stability of perovskite solar cells.

DEDICATION

This thesis is dedicated to God almighty for seeing me through this program in good health and sound mind and also for divine wisdom and understanding throughout the course of the research.

To my lovely mother, Mrs. Eunice O. Obi and wonderful siblings, Obi Ijeoma, Obi Kenechukwu and Obi Chidinma, for their encouragement, Concern and help (both financially and otherwise) all through my stay at AUST.

ACKNOWLEDGEMENT

I will like to express my profound gratitude to my supervisor Dr Abdulhakeem Bello, under whose tutelage and encouragement, I was able to complete this research. I would also want to thank Mr. Dahiru Sanni, for his tireless efforts and guidance from the conception of this work to its full realization. I also acknowledge the efforts of Prof. Marc Burgelman and his co-workers, Department of Electronics and Information Systems, University of Gent, Belgium for the development of the SCAPS software package and allowing its use. Finally, I want to appreciate my family, friends, colleagues and the entire AUST community for their immeasurable assistance and support throughout the course of my study and research in the University.

TABLE OF CONTENTS

TITLE PAGE	i
CERTIFICATION.....	ii
ABSTRACT.....	iv
ACKNOWLEDGEMENT.....	vi
LIST OF TABLE	x
LIST OF FIGURES	xi
CHAPTER ONE	1
INTRODUCTION.....	1
1.1 BACKGROUND OF THE STUDY.....	1
1.2 MOTIVATION	2
1.3 OBJECTIVES	3
CHAPTER TWO	4
2.1 LITERATURE REVIEW.....	4
2.1.1 RADIATION FROM THE SUN.....	4
2.1.2 SOLAR ENERGY	4
2.2 THE SOLAR CELL	6
2.3 GENERATIONS OF SOLAR CELL	7
2.3.1 THE FIRST GENERATION	7
2.3.2 THE SECOND GENERATION	8
2.3.3 THE THIRD GENERARATION	8
2.4 PEROVSKITE	9
2.4.1 CHARGE TRANSPORT IN PEROVSKITE SOLAR CELLS (PSC).....	10
2.4.2 FABRICATION OF PEROVSKITE SOLAR CELLS (PSCs).....	12
2.5 SOLAR CELL PHYSICS.....	13
2.5.1 SEMICONDUCTORS	13
2.5.2 BAND GAP.....	13
2.5.3 ABSORBANCE AND ABSORPTION COEFFICIENT	15
2.5.4 DENSITY OF STATE	16
2.5.5 CARRIER CONCENTRATION	16
2.5.6 DOPING.....	17
2.6 P-N JUNCTION	18
2.7 SOLAR CELL PARAMETERS	19
2.8 TRANSPORT PHENOMENA IN SEMICONDUCTORS.....	21
2.9 RECOMBINATION	22

2.9.1	NON-RADIATIVE RECOMBINATION	22
2.9.2	BAND-TO-BAND RADIATIVE RECOMBINATION	22
2.9.3	AUGER RECOMBINATION.....	22
2.9.4	SURFACE RECOMBINATION	23
2.10	LOSS MECHANISMS	23
2.10.1	LOSS DUE TO SPECTRAL MISMATCH	23
2.10.2	OPTICAL LOSSES	23
2.10.3	THE RECOMBINATION LOSS	24
2.10.4	THE SERIES AND SHUNT RESISTANCE LOSS.....	24
CHAPTER THREE.....		25
3.1	SIMULATION PROCEDURE	25
3.1.1	AMPS 1-D.....	25
3.1.1.1	ADVANTAGES OF AMPS 1-D.....	25
3.1.1.2	DISADVANTAGES OF AMPS 1-D.....	26
3.1.2	PC1D	26
3.1.2.1	ADVANTAGES OF PC1D.....	26
3.1.2.2	DISADVANTAGES OF PC1D	26
3.1.3	wxAMPS	26
3.1.3.1	ADVANTAGES OF wxAMPS.....	26
3.1.3.2	DISADVANTAGES OF wxAMPS	27
3.1.4	SCAPS 1-D.....	27
3.1.4.1	ADVANTAGES OF SCAPS 1-D	27
3.1.4.2	DISADVANTAGES OF SCAPS 1-D.....	27
3.2	SCAPS 1-D INTERFACE.....	28
3.2.1	THE WORKING POINT	28
3.2.2	THE ACTION POINT.....	29
3.2.3	LAYER PROPERTIES SPECIFICATION	29
3.2.4	RESULTS OBTAINABLE.....	30
CHAPTER FOUR.....		31
4.1	DESIGN AND SIMULATION	31
4.2	DEVICE ARCHITECTURE	31
4.3	SIMULATION PARAMETERS	31
4.4	RESULTS AND DISCUSSION	33
4.4.1	EFFECT OF ABSORBER LAYER THICKNESS	33
4.4.2	EFFECT OF ORGANIC AND INORGANIC TRANSPORT LAYERS	39

4.4.3	EFFECT OF TEMPERATURE	40
CHAPTER FIVE		47
5.1	CONCLUSION	47
5.2	RECOMMENDATION.....	47
REFERENCES.....		48

LIST OF TABLE

Table 1: Showing the different electrical properties of the proposed solar cell layers for simulation.....	32
Table 2: Variation of cell characteristics with thickness for CuI/(CH ₃ NH ₃) ₃ Bi ₂ I ₉ /ZnO	Error!
Bookmark not defined.	
Table 3: Variation of cell characteristics with thickness for Cu ₂ O/(CH ₃ NH ₃) ₃ Bi ₂ I ₉ /ZnO	Error!
Bookmark not defined.	
Table 4: Variation of cell characteristics with thickness for Cu ₂ O/(CH ₃ NH ₃) ₃ Bi ₂ I ₉ /TiO ₂	35
Table 5: Absorber of cell characteristics with thickness for CuI/(CH ₃ NH ₃) ₃ Bi ₂ I ₉ /TiO ₂	36
Table 6: Variation of cell characteristics with thickness for SPIRO-OMETAD/(CH ₃ NH ₃) ₃ Bi ₂ I ₉ /PCBM	37
Table 7: Variation of cell characteristics with thickness for SPIRO-OMETAD/(CH ₃ NH ₃) ₃ Bi ₂ I ₉ /P ₃ HT.....	Error! Bookmark not defined.
Table 8: Different cell structures and their corresponding cell characteristics.....	40
Table 9: Variation of cell characteristics with temperature for CuI/(CH ₃ NH ₃) ₃ Bi ₂ I ₉ /ZnO	40
Table 10: Variation of cell characteristics with temperature for Cu ₂ O/(CH ₃ NH ₃) ₃ Bi ₂ I ₉ /ZnO	41
Table 11: Variation of cell characteristics with temperature for Cu ₂ O/(CH ₃ NH ₃) ₃ Bi ₂ I ₉ /TiO ₂	42
Table 12: Variation of cell characteristics with temperature for CuI/(CH ₃ NH ₃) ₃ Bi ₂ I ₉ /TiO ₂	43
Table 13: Variation of cell characteristics with temperature for SPIRO-OMETAD/(CH ₃ NH ₃) ₃ Bi ₂ I ₉ /PCBM	44
Table 14: Variation of cell characteristics with temperature for SPIRO-OMETAD/(CH ₃ NH ₃) ₃ Bi ₂ I ₉ /P ₃ HT.....	45

LIST OF FIGURES

Fig. 1: Drastic increase in power conversion efficiency of perovskite solar.	2
Fig. 2: Distribution of solar spectra entering the lower parts of the atmosphere	5
Fig. 3: Solar Cell working principle.	6
Fig. 4: Typical silicon solar cell	8
Fig. 5: Structure of perovskites.....	9
Fig. 6: Charge transport in perovskite solar cells	10
Fig. 7: (a) Direct band gap semiconductor	14
Fig. 7: (b) Indirect band gap semiconductor.....	14
Fig. 8: The p-n junction, the space charge region (depletion zone).....	19
Fig. 9: The I-V characteristics of a solar cell	20
Fig. 10: Flow chart for the operation of the SCAPS 1-D.....	28
Fig. 11: Panel of the SCAPS 1-D software.....	28
Fig. 12: Solar cell definition panel.....	29
Fig. 13: Layer properties panel, for specifying the properties of the layers that make up the device.	30
Fig. 14: Proposed cell structure with single bismuth-based absorber layer.....	31
Fig. 15: Absorber thickness vs efficiency for $\text{CuI}/(\text{CH}_3\text{NH}_3)_3\text{Bi}_2\text{I}_9/\text{ZnO}$	34
Fig. 16: absorber thickness vs efficiency for $\text{Cu}_2\text{O}/(\text{CH}_3\text{NH}_3)_3\text{Bi}_2\text{I}_9/\text{ZnO}$	35
Fig. 17: Absorber thickness vs efficiency for $\text{Cu}_2\text{O}/(\text{CH}_3\text{NH}_3)_3\text{Bi}_2\text{I}_9/\text{TiO}_2$	36
Fig. 18: Absorber thickness vs efficiency for $\text{CuI}/(\text{CH}_3\text{NH}_3)_3\text{Bi}_2\text{I}_9/\text{TiO}_2$	37
Fig. 19: Absorber thickness vs efficiency for SPIRO-OMETAD/ $(\text{CH}_3\text{NH}_3)_3\text{Bi}_2\text{I}_9/\text{PCBM}$	38
Fig. 20: Absorber thickness vs efficiency for SPIRO-OMETAD/ $(\text{CH}_3\text{NH}_3)_3\text{Bi}_2\text{I}_9/\text{P}_3\text{HT}$	39
Fig. 21: Temperature vs efficiency for $\text{CuI}/(\text{CH}_3\text{NH}_3)_3\text{Bi}_2\text{I}_9/\text{ZnO}$	41
Fig. 22: Temperature vs efficiency for $\text{Cu}_2\text{O}/(\text{CH}_3\text{NH}_3)_3\text{Bi}_2\text{I}_9/\text{ZnO}$	42
Fig. 23: Temperature vs efficiency for $\text{Cu}_2\text{O}/(\text{CH}_3\text{NH}_3)_3\text{Bi}_2\text{I}_9/\text{TiO}_2$	43
Fig. 24: Temperature vs efficiency for $\text{CuI}/(\text{CH}_3\text{NH}_3)_3\text{Bi}_2\text{I}_9/\text{TiO}_2$	44
Fig. 25: Temperature vs efficiency for SPIRO-OMETAD/ $(\text{CH}_3\text{NH}_3)_3\text{Bi}_2\text{I}_9/\text{PCBM}$	45
Fig. 26: Temperature vs efficiency for SPIRO-OMETAD/ $(\text{CH}_3\text{NH}_3)_3\text{Bi}_2\text{I}_9/\text{P}_3\text{HT}$	46

CHAPTER ONE

INTRODUCTION

1.1 BACKGROUND OF THE STUDY

The demand for energy in the ever-growing population and increasing economy cannot be overemphasized. It is no news that the energy needed to survive comes in different forms, with different modes of production which has advanced over years. Energy can be from renewable and non-renewable sources. Renewable energy refers to those whose sources that can be replenished naturally with time, and includes, Solar, Hydro, Geothermal heat, Wind, Waves, etc. Non-renewable energy refers to those that cannot be replenished naturally to keep up with the rate of consumption, they include; oil, coal, natural gas, nuclear power. As a result of the depletion of the non-renewable sources of energy, and its respective environmental hazards, that is, the release of green-house gases which can cause environmental pollution, global-warming, and the safety concerns associated with the use of nuclear power, it is necessary to make use of clean, renewable sources for energy production. In the quest for a clean, renewable and reliable source of energy, solar energy has evolved as a very promising area with its rapid development in technology, cost minimization and accessibility. [1]

There is enormous supply of energy from the sun in the form of heat and radiations, at no cost and limit, on a daily basis [2]. Harnessing this energy from the sun has been fostered by the development of photovoltaic technology, although faced with some challenges of low cost, improved performance, stability and reliability. Tremendous research is ongoing in this area as it possesses a huge potential for solving the world energy need. Over the years, silicon solar cells have been the dominant photovoltaic technology. M. Fridolf reported that silicon cell was first experimentally used as a primary power source for a repeater of the Bell System type P rural carrier in October, 1955 [3]. Though Silicon solar cells have shown to have high efficiency, and lasts long, there exists some disadvantages to the silicon based technology. Some of which includes;

- High cost of manufacturing.
- Risk of losing some of their efficiencies at high temperatures

As a result of these, the thin-film technology is adopted, and perovskite solar cells emerged as very promising as it has shown drastic increase in efficiency over a short period of time. Figure 1 shows this increase as reported by Ossila with data from NREL (National Renewable Energy Laboratory) [4].

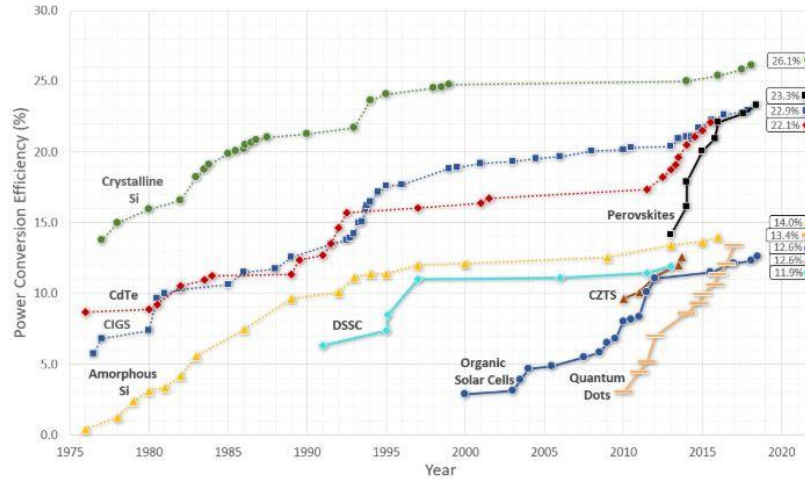


Fig. 1: Drastic increase in power conversion efficiency of perovskite solar cell in a short time from 2012.

1.2 MOTIVATION

As a result of the combination of lower cost, high efficiency and simpler processing method, lead based perovskite (methylammonium lead triiodide) solar cells have attracted significant attention [5]. In recent years, it was reported that the power conversion efficiency of the lead-based perovskite has tremendously increased from 3.8 % in 2009 [5], to exceeding over 21 % in 2018 [6]. Despite these, the toxicity of lead could be an impediment for commercialization, and large-scale fabrication and use ascribable to its environmental threat. This has led to research into replacing the water-soluble lead with other materials such as tin. The low band gap of Tin perovskite (methylammonium tin triiodide) compared to the lead based, makes it have a higher absorption range for sunlight, and has recorded a high theoretical power conversion efficiency of 26.05 % [6], but has a problem of instability as the Sn (II) readily oxidizes to Sn (IV) in atmospheric exposure [7]. It is seen that bismuth element of the 6-p block, which has outer lone pair of $6s^2$ electron like Pb and non-toxic [8], hence the desire to opt for investigating into the

use as possible Pb replacement in organic-inorganic halide perovskite solar cells. Also, since perovskite faces stability challenges, this work looks at the effect of replacing the organic charge carriers with their inorganic counterparts.

1.3 OBJECTIVES

1. To replace lead with bismuth for perovskite fabrication
2. To improve perovskite stability by replacing organic charge carriers with inorganic charge carriers.
3. To investigate the effects of variation of temperature and absorber thickness on different types of device architectures

CHAPTER TWO

2.1 LITERATURE REVIEW

2.1.1 Radiation from the Sun

According to NASA Solar System Exploration, the sun is the closest star to the earth as there are lots of stars, hence its name, “yellow dwarf star”. It is about 4.5 billion years in age, and a distance of about 26,000 light years from the galactic center. It is 109.2 times larger than the earth, with an equatorial radius of 695,508km, and density of 1.409g/cm^3 . It is referred to as a hot ball of glowing gasses, made up of 92.1 percent hydrogen and 7.8 percent helium held together by its own gravity. Its gravity is also responsible for holding the solar system together, keeping it all in its orbit from the biggest planets to the smallest debris. In its orbit there are eight planets, at least five dwarf planets, tens of thousands of asteroids, and up to three trillion comets and icy bodies. The sun makes up 99.8 percent of the entire solar system. A magnetic field is generated by the electric currents in the sun, and is carried out by the solar wind through the solar system. At its poles, the rotation of the sun is once at every 35 earth days on its axis, but spins once about every 25days at the equator. The core of the sun is about 27 million degrees Fahrenheit (15 million degrees Celsius). In fact there will be no life on earth without the high energy from the sun as the seasons, ocean currents, weather, climate, radiation belts and aurorae, are driven by the connection and interactivity between the sun and earth [9].

2.1.2 Solar Energy

Solar energy is a clean, renewable energy derived from the sun in the form of light and heat, although, only a small fraction reaches the earth. This solar energy is radiated by electromagnetic waves from the sun over a wavelength range known as the solar spectrum and lies in three major regions: ultraviolet, visible, and infrared. The spectrum spans from about 290nm in the ultraviolet (UV) region to over 3,200nm in the far infrared region [10]. The range of energies of the radiation from the sun that reaches the top of the atmosphere of the earth is referred to as the spectral distribution and shown in the figure 2 [10]. The range of wavelengths in the solar spectrum is represented on the X-axis (measured in nanometers), whilst the amount of power (watts) falling per unit area just outside the earth’s atmosphere is represented on the Y-axis [10].

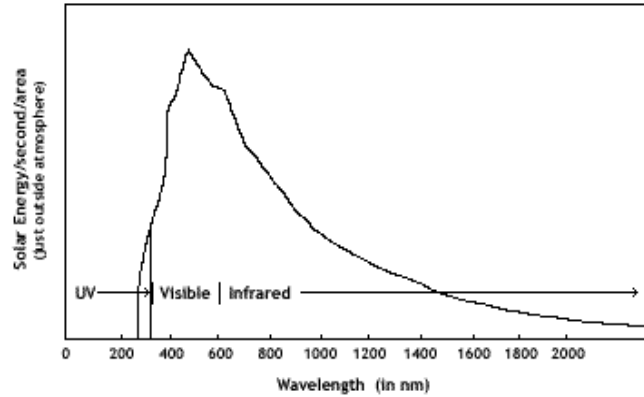


Fig. 2: Distribution of solar spectra entering the lower parts of the atmosphere [10]

From the figure, it can be seen that most of the energy coming from the sun lies in the visible region, making up what is called Sunlight (white light) [10]. At the Earth's surface, atmospheric effects have various impacts on the radiation of the sun. These effects include absorption and scattering of the radiation by atmospheric gases, and dusts. Ozone gases(O_3), carbon dioxide (CO_2), and water vapor (H_2O), absorb photons with energies close to their bond energies [11]. This absorption and scattering of light as a result of the air molecules and dust present in the atmosphere, is the major cause of the reduction in power from solar radiation. One term that quantifies this solar light power reduction is referred to as the air mass. It is the normalization of the path length which light takes through the atmosphere to the shortest possible path length [11]. The Air Mass is defined as;

$$AM = \frac{1}{\cos(\theta)}$$

Here, θ is the zenith angle, that is, the angle from the vertical.

The variations in power and spectrum of the incident light greatly affects the efficiency of the solar cell. For accuracy, a standardized spectrum at the Earth's surface is set as AM1.5G, where G stands for global, and includes both direct and diffuse radiation, and has been normalized to 1 kW/m^2 [11].

2.2 THE SOLAR CELL

The solar cell is referred to as a device that directly converts energy from the incident radiation from the sun to electricity. It is also known as a photovoltaic (PV) cell [12], hence its working principle is the photovoltaic effect. Klaus Jäger et al. reported that in a solar cell, the photovoltaic effect can be divided into three basic processes [13];

1. Absorption of photons leading to charge carrier generation
2. Separation of photo-generated charge carriers at the junction
3. Collection of photo-generated charge carriers at the contacts

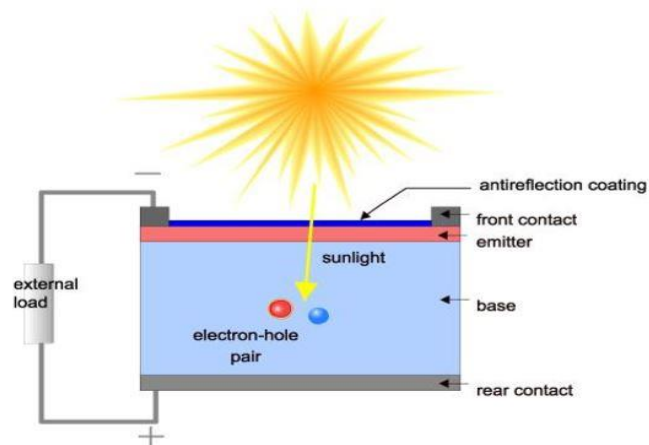


Fig. 3: Solar cell working principle

When the rays from the sun strikes the solar cell, absorption of the light occurs. This absorption is subject to the band gap (E_g), of the semiconducting absorber. If the energy of the incident photon is equal to, or greater than the band gap of the material, absorption occurs, otherwise, it will just be transmitted through the material [14]. The absorption of these photons generates an electron-hole pairs in the cell, and to avoid their recombination, selective membranes, also known as charge transport materials (formed by n and p-type materials), are placed on both sides of the absorbing layer, so that the generated electron and holes are separated. In order for these charge carriers to work in an external circuit, they are being collected by electrical contacts, where the electrons are collected by the 'front contact' and the holes by the 'back contact' as seen in the figure 3 [13].

2.3 GENERATIONS OF SOLAR CELL

Kiran Ranabhat et. al. reported three generations of the solar cell, that is, the first, second and third generations [15].

2.3.1 THE FIRST GENERATION

This generation represents the earliest types of solar cells made from silicon. This generation of solar cells are produced on wafers [16]. The silicon solar cells are currently the most used technology, because of its high efficiency. There are two layers that make up the silicon solar cell- a p-type (positive) layer, and an n-type (negative) layer [15]. The p-type layer is usually made by doping the silicon with a trivalent element, resulting in creation of extra holes in the crystal lattice, whilst the n-type is made by doping the silicon with a pentavalent element, resulting in the creation of extra electrons in the crystal lattice. Depending on the method of production of the wafer, there are three different types of silicon cells used.

- Monocrystalline silicon solar cell (Mono c-Si)
- Polycrystalline silicon solar cell (Poly c-Si)
- Amorphous silicon solar cell

The monocrystalline silicon solar cell as the name implies, is a solar cell made by a single silicon crystal. This technology has shown very high efficiency, and can be due to the high level of purity of the silicon wafer. These single crystal silicon wafers are made by the Czochralski process [15]. The main disadvantage of this type is the high cost of production, due to the techniques required in obtaining the single crystal.

The polycrystalline and amorphous silicon solar cells are not as pure as the monocrystalline, and as such, have lower efficiencies, though with lower cost of production. Generally, the issue with this generation of solar cells is the high cost, amount of materials used.

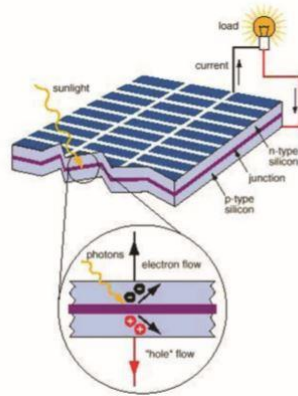


Fig. 4: Typical silicon solar cell [15]

2.3.2 THE SECOND GENERATION

This can be called the thin-film generation. It was developed to address the issue of high cost in the first generation. Cost here is reduced by reduction in the amount of materials used, and the processing technique adopted [15]. Unlike the first-generation types that are produced on wafer, these ones are produced on substrates (such as glass, metal, or polymers). Their production techniques include; vapor deposition, electroplating and use of ultrasonic nozzles [17]. Examples of the second-generation solar cells are; Amorphous Silicon (a-Si), Cadmium-Telluride (CdTe), copper-indium-selenide (CIS) and copper-indium-gallium-diselenide (CIGS). The thin film cells also rely on the p-n junction design, and are made of layers of different band gap, with the top layer having a higher band gap to absorb higher energy photons, whilst the bottom layer have a lower band gap to absorb lower energy photon [15]. One main concern of this generation of solar cells is that their main materials are increasingly becoming rare and expensive (e.g. indium), and some are toxic (e.g. Cadmium) [15].

- Cadmium Telluride
- Copper Indium Gallium di-Selenide

2.3.3 THE THIRD GENERATION

This generation of solar cells tackles the issues of high cost poised by the first generation, and the low availability and toxicity of materials of the second generation [15]. Research into this generation of solar cells to enhance electrical performance at a low cost is still ongoing. It looks

at polymer based solar cells, dye sensitized solar cells, nanocrystal based solar cells, and concentrated solar cells [16].

- Dye Sensitized Solar Cells
- Nanocrystal based Solar Cells
- Concentrated Solar Cells
- Polymer based Solar Cells

2.4 PEROVSKITE

Perovskite is a generic name referring to materials that exhibits the same crystal structure as calcium titanate, that is, AXB_3 [18]. It was named after the Russian mineralogist Count Lev Aleksevich von Petrovski, after being discovered by the Prussian mineralogist Gustav Rose in 1839, in mineral deposits in the Ural Mountains [19]. This structure is adopted by so many minerals, exhibiting different properties including piezoelectric, semiconducting, insulating, conducting, thermoelectric, antiferromagnetic, and superconducting [18]. In the AXB_3 structure of perovskites, the A and B are two different sized cations, bonded by the anion X [20]. In the structure of perovskite shown in, figure 5, the A cation is larger than the B cation, and lies between the octahedra of X anions that surrounds the B cation [20].

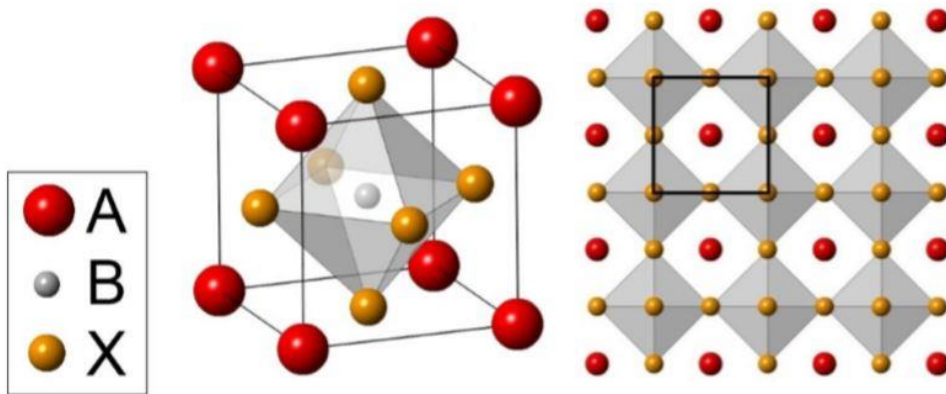


Fig. 5: AXB_3 structure of perovskites

Irrespective of the fact that there exist many minerals with the AXB_3 structure, only few are suitable to be used in solar cells as efficient light absorbers due to requirements like suitable

bandgap, high mobility, long charge carrier lifetime, and band alignment with surfaces in contact with it. High bandgaps in perovskites is not suitable for photovoltaic applications because of their divalent anions [21]. The perovskite currently in use now are the organic-inorganic hybrid system. When viewed as a mineral with the AXB_3 crystal structure, the X represents the monovalent halide anion(Cl, Br, I, etc.), B represents a divalent cation, which can be, Pb^{2+} , Sn^{2+} , Bi^{2+} , etc. whilst the A represents the organic cation, which is mostly methylammonium or formamidinium, $CH_3NH_3^+$ or $NH_2CH_3NH_2^+$ respectively [22]. The most commonly used organic-inorganic hybrid perovskite is the methylammonium lead halide $CH_3NH_3PbI_3$ (or Cl, nor Br.) also known as $MAPbI_3$. This type of perovskite gained recognition because of the rapid increase in its conversion efficiency in a short period of time, due to its improved fabrication processes [23].

2.4.1 CHARGE TRANSPORT IN PEROVSKITE SOLAR CELLS (PSC)

The mechanism of charge transport in PSCs is different from others because of the nature of its active layer materials. The perovskite absorbing material, $MAPbI_3$, is positioned in between two transport layers (i.e. the electron and hole transport layers, ETL and HTL respectively), with a front transparent electrode, and a back-metal electrode.

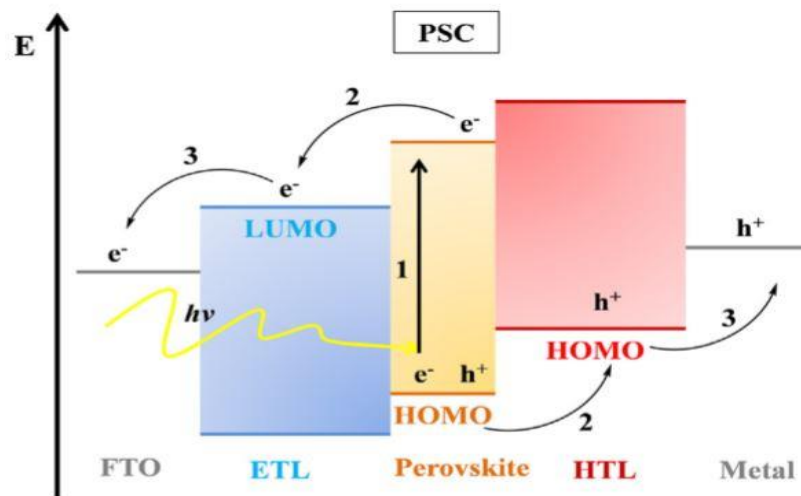


Fig. 6: Charge transport in perovskite solar cells

As clearly shown in the figure 6 above, stage 1 shows the absorption of photons by the perovskite material, and the subsequent excitation of electrons from the highest occupied molecular orbital (HOMO), to the least unoccupied molecular orbital (LUMO). The second (2) stage shows the collection of generated electrons and holes by the ETL and HTL respectively. The third (3) stage shows the extraction of charges by the front and back contact electrodes. It is important to note that the valence and conduction band, which are equivalent to the HOMO and LUMO, of the MAPbI_3 are formed by the Pb and I orbitals, whilst the MA do not partake electronically in the band structure, but influences the optical properties as it governs the formation of the 3D perovskite crystal. With this, it shows that one can successfully tweak the optical and electronic properties of the PSCs, which has been one of the brighter sides of these type of solar cells [23].

Rui Sheng et al conducted an experiment, where they substituted the iodine in the MAPbI_3 , to bromine, making it MAPbBr_3 . They found out that the band gap which was at 1.55 eV increased to about 2.3 eV, with a high voltage potential, suggesting that it is suitable for tandem solar cell applications [24]. This shows that the optical properties of the perovskite layer can be tuned. Jun Hong Noh et al performed an experiment by chemically tuning the perovskite material to a mixed halide structure, i.e., having incorporating both the iodine and bromine in it ($\text{MAPb(I}_{1-x}\text{Br}_x)_3$). The solar cell exhibited a high-power conversion efficiency of 12.3 % and better stability, and they also showed that the electrical properties can be adjusted. Similarly, Noel et al in 2014 performed an experiment on lead-free tin perovskite, $\text{CH}_3\text{NH}_3\text{SnI}_3$, and reported an efficiency of 6 %, low stability, with mobility of $16 \text{ cm}^2 \text{ V}^{-1} \text{ s}^{-1}$, but with low voltage losses, showing that the efficiency can be improved by exploiting its potentials [25]. Jung et al reported efficiencies between 0.03 to 0.035 % using co-evaporation deposition method, and higher efficiencies of 1.12% with sequential deposition method for $\text{CH}_3\text{NH}_3\text{SnBr}_3$ planar perovskite solar cells. This shows the processing technique can affect the efficiency of the perovskite solar cell [26].

Harikesh et al. experimented on solution processed antimony-based perovskite solar cell, $\text{Rb}_3\text{Sb}_2\text{I}_9$, and reported a V_{oc} of 0.55V, a J_{sc} of 2.12 mA cm^{-2} , an FF of 57%, and an efficiency of 0.66% [27]. Ashish Kulkarni et al. investigated bismuth-based perovskite solar cell, $(\text{CH}_3\text{NH}_3)_3\text{Bi}_2\text{I}_9$ by adding small amount of N-methyl-2-pyrrolidone (NMP) to control the

morphology, and reported that the device showed an efficiency of 0.31 % with high reproducibility, and high stability for about 30 days on exposure to ambient air [7]. Eckhardt et al. reported the crystallographic nature of bismuth perovskites, $(\text{CH}_3\text{NH}_3)_3(\text{Bi}_2\text{I}_9)$, and hinted that they contain isolated $\text{Bi}_2\text{I}_9^{3-}$ anions, and not contain corner sharing octahedral that is normally observed in most perovskite. The possibility of obtaining a highly pure and crystalline phase $(\text{CH}_3\text{NH}_3)_3\text{Bi}_2\text{I}_9$ was shown, and an open circuit voltage of 800 mV but low efficiency was reported.

2.4.2 FABRICATION OF PEROVSKITE SOLAR CELLS (PSCs)

There are various techniques of fabricating thin film PSCs, but the best methods reported are solution-based deposition, and vapor-assisted deposition [28]. The perovskite layer of the solar cell can be fabricated either by one-step deposition, or by two-step deposition [29]. The one-step layer fabrication process deals with preparation of a solution of the perovskite precursors, spin-coating, and annealing in the range of 100-150 °C. The precursor is prepared from the organic and inorganic halides [29].

The two-step layer fabrication method requires the separate deposition of the organic halide, and the inorganic halide [22]. Of the various techniques of fabricating PSCs, the spin coating and spray coating processes will be discussed here, as they are the most widely used.

Spin Coating

It is a solution-based processing technique which is used for depositing the layers of the cell uniformly, and for manufacture of solar cells with small area. This process is simple and cost effective, as one deposits the solution of the layers on the substrate, and it is spin coated, after setting up the spin speed, acceleration, and time of spin coating. These settings also help to optimize the film thickness, and quality of the PSC. One major disadvantage of this type is that uniform films cannot be produced on larger areas [22].

Spray Coating

This solution processing technique is a very efficient and highly scalable in the production of flexible solar cells. It has advantages of rapid film deposition, low processing cost, and can be deposited on large scale for both glass and flexible substrates [28]. In this process, the precursor solution is mixed and placed in the spray coating system. The spray nozzle position and speed are

controlled by software, so as to simulate an industrial process by moving the spray nozzle in a continuous and raster movement [30].

Chemical Vapor Deposition (CVD)

This is one of the most promising vapor deposition techniques for fabrication of thin film PSCs, with uniform thickness, high scalability, and provides better contact between the precursors [29]. In this process, the deposition of perovskite layer is by the transfer of two different co-evaporated precursors that has been heated and mixed, to a substrate that has been preheated with carrier gas, so as to form pin-hole free, uniform films. One disadvantage of this process is that it requires very high vacuum [28].

2.5 SOLAR CELL PHYSICS

This section explains some of the important terminologies associated with photovoltaics.

2.5.1 SEMICONDUCTORS

Semiconductors are materials whose conductivity lies between those of conductors and insulators. Conductors allow the easy flow of electricity through them, insulators do not allow the flow of electricity through them, whilst electricity pass through semiconductors under certain conditions [31]. Semiconductors can be a pure element (silicon, germanium, etc.), or a compound (Gallium-Arsenide, Indium-Phosphate, etc.). A semiconductor can be intrinsic or extrinsic. An intrinsic semiconductor is referred to as a pure semiconductor, that is, the absence of impurities. Whilst an extrinsic semiconductor is one that has been selectively doped with impurity atoms. When the semiconductor is doped with a pentavalent element (e.g. Phosphorus), it is called an N-type semiconductor. When doped with a trivalent element (e.g. Boron), it is called a P-type semiconductor. N-type semiconductors have excess electrons in their crystal structure, whilst P-type has excess holes.

2.5.2 BAND GAP

The use of a semiconductor as an optoelectronic device requires; adequate knowledge of its band structure. The band gap of a semiconductor is the distance between the conduction band and the valence band. The valence band is the lowest energy band of a semiconductor. It is usually filled with electrons at room temperature, and resulting to no conductivity. When the temperature is increased, depending on the level of excitation, the electrons jump from the valence band to the

conduction band, hence conductive. If the energy of excitation is larger than the band gap, then electrons will successfully jump from the valence band to the conduction band (excitation).

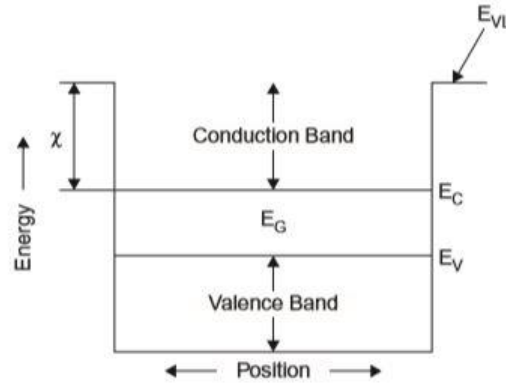


Figure 2.6 Energy band diagram of a semiconductor [32]

When the maximum energy of the valence band of a semiconductor lies on the same K-value as the minimum energy of the conduction band (that is, having the same wave vector), then that semiconductor is said to have a direct band gap. But when the maximum of the valence band, and the minimum of the conduction band lies on different k-values, then the semiconductor has an indirect band gap.

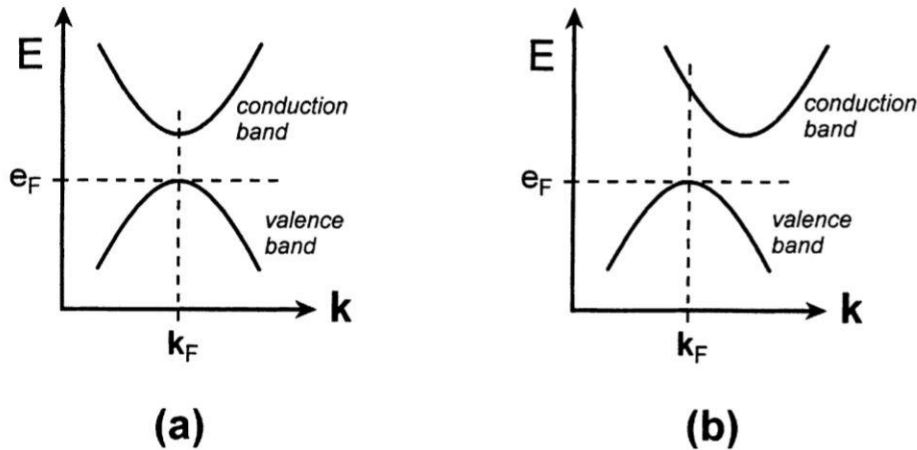


Fig. 7: (a) Direct band gap semiconductor (b) Indirect band gap semiconductor [33]

2.5.3 ABSORBANCE AND ABSORPTION COEFFICIENT

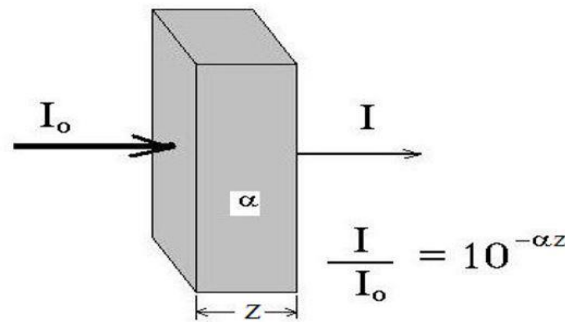
As stated earlier, the absorption of the incident photon from the sun depends on the energy of the photon, and the band gap of the material. Absorption in semiconductors can occur in different processes: Free carrier absorption, band-to-band absorption, and others [32]. The free carrier absorption is a form of intra-band absorption, in that, the electrons or holes are excited with photons to a higher energy level within the same band. In band-to-band transition, electrons are excited by photons from the valence band to the conduction band [32]. For Optoelectronic devices, this band-to-band transition is the most important interaction between the semiconductor and the incident photon [34]. Which leads to the creation of electron-hole pairs, and subsequent conversion to electricity [35].

A materials absorption coefficient (α) is a property of a material that indicates the depth to which light of a particular wavelength penetrates that material, before its being absorbed [11]. The absorption coefficient of a material largely depends on the wavelength (λ), and is related to the extinction coefficient (k) as [36];

$$\alpha = \frac{4\pi k}{\lambda} \dots \dots \dots (1)$$

The extinction coefficient (k) is the imaginary part of a complex refractive index. That is [36];

$$N = n - ik \dots \dots \dots (2)$$



The absorption coefficient of a material is also related to the intensity of the light as [37];

$$I(z) = I_0 e^{-\alpha z} \dots \dots \dots (3)$$

Where; I_0 = intensity of the incident light

$I(z)$ = the intensity of light transmitted

Z = the transmission distance

α = absorption coefficient of the material

2.5.4 DENSITY OF STATE

The density of state is the number of allowable electronic states an electron occupies at a particular energy level per unit volume per unit energy. Physical properties of materials like optical absorption, largely depends on the number of allowed states present [34]. This current deals with the flow of charge and, the knowledge of the number of available charges (carriers) is very important. This number of available charges depends on the number of available energy states [35]. The density of state is related to the energy as [35];

$$g(E) = \frac{4\pi(2m)^{3/2}}{h^3} \sqrt{E} \dots \dots \dots (4)$$

This expression shows that the number of available electronic state is dependent on the energy of the free electron. This tells us that as the energy decreases, the number of available states also decreases. The probability of occupation of an electronic state by an electron is called the Fermi-Dirac distribution $f_F(E)$ [35].

$$f_F(E) = \frac{1}{1 + \exp\left(\frac{E - E_f}{kT}\right)} \dots \dots \dots (5)$$

2.5.5 CARRIER CONCENTRATION

This refers to the number of electrons or holes present in a semiconductor for charge transport. The knowledge of the concentration of these carriers helps in understanding how a semiconductor device works. One can get the total concentration of electrons (n) in the conduction band, and holes (p) in the valence band by multiplying the density of state function with the distribution probability function, and integrating over the entire energy band [13].

$$n = \int_{E_c}^{E_{top}} g(E) f_F(E) dE \dots \dots \dots (6)$$

$$p = \int_{E_{bottom}}^{E_v} g(E) [1 - f_F(E)] dE \dots \dots \dots (7)$$

By substituting the values of $g(E)$ and $f_F(E)$ into the expressions above will give the carrier concentrations as [13]:

$$n = N_C \exp\left(\frac{E_F - E_C}{kT}\right) \dots \dots \dots (8)$$

$$p = N_V \exp\left(\frac{E_V - E_F}{kT}\right) \dots \dots \dots (9)$$

Where; N_C is the effective density of state of the conduction band, and is given as [38]:

$$N_C = 2 \left(\frac{2\pi m_e^* kT}{h^2}\right)^{3/2} \dots \dots \dots (10)$$

N_V is the effective density of state of the conduction band, and is given as [38]:

$$N_V = 2 \left(\frac{2\pi m_h^* kT}{h^2}\right)^{3/2} \dots \dots \dots (11)$$

2.5.6 DOPING

This is a method of increasing the number of charge carriers in a semiconductor [39]. This is achieved by introducing impurities to the semiconductor lattice, forming an extrinsic semiconductor [38]. With this process of doping, one can be able to manipulate the concentrations of electrons and holes in a semiconductor at will [13]. In this process of doping, the atoms of the impurity element (dopant), substitutes the atoms of the semiconductor in the crystal lattice [13]. Doping of a semiconductor can be done with an atom with three valence electrons, or one with five valence electrons. When a semiconductor lattice, for example silicon (with four electrons), is doped with a trivalent element (three valence electrons), it is called a P-type doped semiconductor. Some of these trivalent elements are boron (B), aluminum (Al), indium (In), or gallium (Ga) [39]. When these elements are introduced into the silicon (Si) semiconductor lattice with four neighboring atoms, there exists a missing electron in one of the bonds, resulting in what is referred to as the creation of a hole [38] and a positive charge cloud around the impurity atom in the crystal [39]. However, as a result of this missing electron to complete the bonding of the impurity atom to the Si semiconductor atoms, it readily accepts

electrons from neighboring Si-Si bonded atoms, hence, creating a hole capable of moving about the lattice [13]. The concentration of these holes increases as more of this trivalent dopant are used, thereby increasing the concentration of acceptors, and is denoted by N_A [13].

When the Si semiconductor lattice is doped with an impurity with five valence electrons, it is called an N-type doped semiconductor. Examples of this impurity atoms are phosphorus (P), arsenic (As), antimony (Sb) or bismuth (Bi) [39]. When any of these impurity atoms is introduced to the Si lattice, it pairs with the four atoms of the Si, leaving one extra atom of the dopant element, which is loosely bound [39]. This loosely bound electron is liberated due to the thermal energy available in the Si lattice at room temperature [13], and free to move around the lattice, resulting in extra electrons in the lattice. When more of this impurity dopant is added, the concentration of the extra electrons increases, thereby donating more electrons to the lattice [13]. The impurity atoms are then referred to as donors, and the concentration of donors is represented as N_D [13]. When there is a higher concentration of one type of carrier over the other, we can have what is called majority and minority carriers. Majority carriers refer to holes in a P-type semiconductor, and electrons in an N-type semiconductor, whilst minority carriers refer to holes in an N-type semiconductor, and electrons in a P-type semiconductor [13].

2.6 P-N Junction

This is a junction formed at the interface of a P-type and an N-type semiconductor in contact [40]. The junction can be formed by diffusion of the different doping elements on the semiconductor material (e.g. diffusion of Boron on a Bismuth doped N-type semiconductor), or by physical or chemical deposition techniques (Epitaxy) [41]. When the P-N junction is formed on the same semiconductor material, then it is called P-N homojunction, but when formed on a semiconducting material such that the N-type material is different from the P-type material, then it is called P-N heterojunction [42]. Also, a P-I-N junction is one in which an intrinsic (I) layer is inserted between the P and N-type layers, and the electric field formed by the p-n junction is stretched across this intrinsic layer [13].

When a p-type and an n-type layer are in contact, without the application of an external voltage, due to the difference in electron concentration between the two layers, electrons from the n-type region diffuse across the p-n junction to the p-type region [13], leaving behind positively charged donor atoms [35]. The difference in hole concentration between these two layers causes

diffusion current of holes from the p-type to the n-type region [13], uncovering negatively charged acceptor atoms [35]. An electric field is induced in the region around the p-n junction from the n to the p side by the net positive and negative charges in the n and p regions [35], which forces the electrons and holes to move in opposite direction than the concentration gradient, resulting in what is called the space charge region (depletion zone) where the forces driving the diffusion of charge carriers across the junction compensates each other, and no net current flows through the p-n junction [13].

A p-n junction allows the flow of current in one bias direction and not in the other, making it a current rectifier [40]. Also, a semiconductor device with a single p-n junction is referred to as a diode.

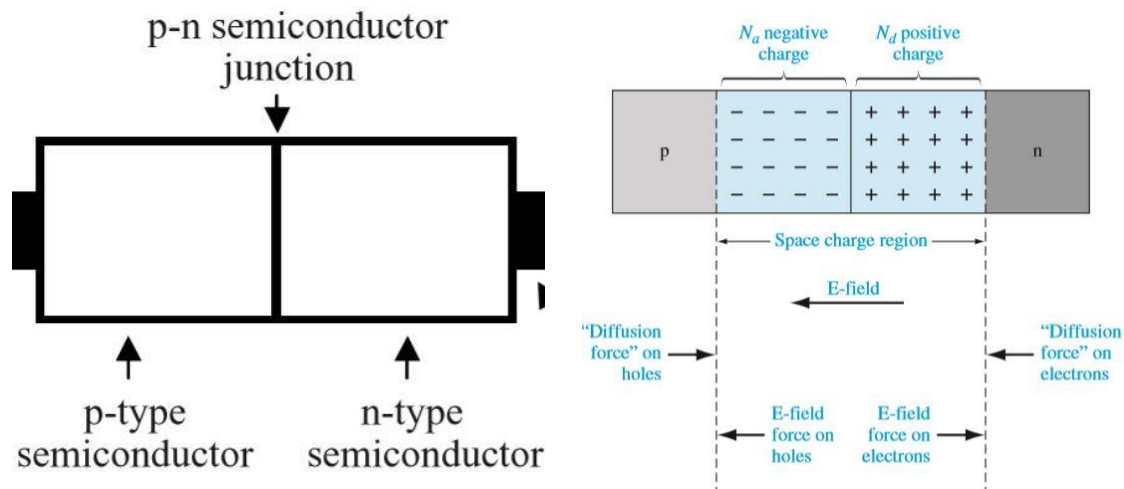


Fig. 8: The p-n junction, the space charge region (depletion zone) [35].

2.7 SOLAR CELL PARAMETERS

There are several important parameters associated with the solar cell. Some of the most important parameters are associated with the efficiency of the solar cell device, viz; short-circuit current density J_{SC} , open-circuit voltage V_{OC} , and fill factor ff , peak power P_{max} [13].

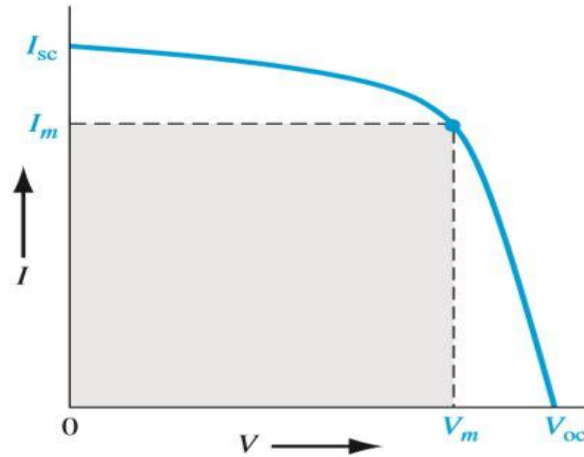


Fig. 9: showing the I-V characteristics of a solar cell [35].

- **Short-Circuit Current Density J_{sc}**

This is referred to as the maximum current produced by the cell when there is no external voltage applied to the cell, and it depends largely on the density of the incident photon flux, determined by the spectrum of the incident light, and the area of the cell [13].

- **Open-Circuit Voltage V_{oc}**

This is the maximum voltage produced by the cell when there is no external current. It depends on the photo-generated current density J_{ph} , and is calculated as [13];

$$V_{oc} = \frac{kT}{e} \ln \left(\frac{J_{ph}}{j_0} + 1 \right) \dots \dots \dots (12)$$

Where j_0 indicates zero net current density.

- **Fill Factor ff**

This is the ratio between the maximum power P_m ($P_m = V_{P_m} * J_{P_m}$) and the product of the V_{oc} and J_{sc} [13].

$$ff = \frac{V_{P_m} * J_{P_m}}{V_{oc} * J_{sc}} \dots \dots \dots (13)$$

Where V_{P_m} and J_{P_m} is the voltage and current density at maximum power respectively [13].

- **Power Conversion Efficiency η**

This is the ratio between the maximum power generated by the cell to the incident power [13].

$$\eta = \frac{P_{max}}{P_{in}} = \frac{J_{P_m} V_{P_m}}{P_{in}} = \frac{J_{sc} * V_{oc} * FF}{P_{in}} \dots \dots \dots (14)$$

2.8 TRANSPORT PHENOMENA IN SEMICONDUCTORS

Here, we take a look at the mechanism of charge transport by the electrons and holes in conductor. The two basic mechanisms are drift and diffusion.

- **Drift**

This is the movement of charged particles due to an electric field. In the presence of an electric field, the holes are accelerated in the direction of the field, whilst the electrons are accelerated in the reverse direction. These charge carrier movements are described by the average drift velocities of the electrons v_{dn} , and holes v_{dp} , and are directly proportional to the electric field E .

$$v_{dn} = -\mu_n E \dots \dots \dots (15)$$

$$v_{dp} = \mu_p E \dots \dots \dots (16)$$

The constant of proportionality, μ , is called the mobility. The carrier mobility characterizes how well the electron and holes will move in the semiconductor due to the electric field. Hence, the drift density of the electron and hole is given as:

$$J_{ndrift} = -en v_{dn} \dots \dots \dots (17)$$

$$J_{pdrift} = en v_{dp} \dots \dots \dots (18)$$

- **Diffusion**

From basic diffusion phenomenon, charged particles move from a region of high concentration to a region of low concentration. For this type of transport phenomenon, the main driving force is the gradient in the particle concentration [13]. Diffusion current density of electrons J_{ndiff} and holes J_{pdiff} are given as;

$$J_{ndiff} = eDn \nabla n \dots \dots \dots (19)$$

$$J_{pdiff} = -eDp \nabla p \dots \dots \dots (20)$$

The terms D_n and D_p refers to the diffusion coefficients of the electrons and holes respectively, and are related to the mobility of the charge carriers by Einstein's relationship as [13];

$$\frac{D_n}{\mu_n} = \frac{D_p}{\mu_p} = \frac{kT}{e} \dots \dots \dots (21)$$

The total diffusion current density, obtained by combining the diffusion currents of electron and hole, is given as [13];

$$J_{diff} = e(D_n \nabla_n - D_p \nabla_p) \dots \dots \dots (22)$$

2.9 RECOMBINATION

The idea of carrier generation in a solar deals with the creation of electron-hole pairs when a semiconductor absorbs photons of energies higher than the band gap has been discussed. The term recombination is an inverse of the generation of excess carriers in the semiconductor. It is the obliteration of excess carriers generated in the semiconductor [42]. The performance of the solar cell strongly depends on the recombination rate as this is capable of reducing the current collected by the solar cell.

There exist different recombination mechanisms, which are briefly discussed as follows;

2.9.1 Non-Radiative Recombination

Here, the recombination occurs within the forbidden gap (between the valence and conduction band), and mostly caused by the presence of localized trap states created by deep level defects in the semiconductor lattice. This type of recombination is also known as Shockley-read-hall recombination. When this recombination occurs, energy is released by vibration of lattice atoms (i.e., Phonon emission) [42].

2.9.2 Band-to-Band Radiative Recombination

This kind of recombination process is an inverse of optical absorption, commonly observed in semiconductors with direct band gap [42], and the energy is released in the form of photons [40].

2.9.3 Auger Recombination

Just as the radiative recombination is mostly peculiar to direct band gap semiconductors, the auger recombination mechanism predominant in semiconductors with indirect band gap [13]. The radiative and non-radiative recombination processes that involves two particles (electron and holes), the auger recombination process involve three particles [13], which includes either electron-electron collisions in the conduction band with subsequent recombination with holes in

the valence band, or hole-hole collisions in the valence band with subsequent recombination with electrons in the conduction band [42]. Hence, we have electron-electron-hole recombination R_{eeh} , or electron-hole-hole recombination R_{ehh} .

2.9.4 Surface Recombination

It is important to note that recombination processes do not only occur at in the bulk of the material, but can also occur at the surface, which is where the periodicity of atoms are interrupted. Hence, the surface recombination rate for electrons and holes is defined as the number, per unit area and per second, of charge carriers vanishing the surface of a semiconductor as a result of recombination mechanisms [40].

2.10 LOSS MECHANISMS

We usually find that the conversion efficiency of ideal solar cells is greater than those of the real solar cells. Hence, there are mechanisms by which energy is lost in the solar cell, and they include;

2.10.1 Loss due to Spectral Mismatch

This type of loss is due to the difference between the photon energy distribution in the solar spectrum and semiconductor material's band gap. As earlier stated, when photons from the sun is incident on the absorber layer of the solar cell, only photons of energy equal to, or greater than the band gap of the absorbing material that gets absorbed, and is capable of generating electron-hole pairs. This means that energy lower than the band gap of the absorbing material is not absorbed, and as such, do not participate in the energy conversion process. Also, in incident photon can carry excess energy, and this excess energy is received by the generated electron and hole pairs, and released as heat in the semiconductor lattice in a process called thermalization. Therefore, these photons with less energy than the semiconductor band gap, and the ones with excess energy larger than the band gap, that are not absorbed, are the main losses of the spectral mismatch phenomena [13].

2.10.2 Optical Losses

This type of loss is mainly characterized by three losses which includes; reflection losses, shading loss and losses due to parasitic absorption [13].

Reflection losses occur as a result of the total reflectance between the solar cell and the surrounding air. This total reflectance is a sum of all the reflections and transmissions that occur at the various interfaces of the solar cell as photons penetrate the cell [13].

Shading losses are as a result of the metal contact (front electrode), at the top of the solar cell which collects electrons from the cell, and transfers to the external load for electricity generation. The area of the cell covered with the metal does not allow light to enter the cell because it slightly absorbs or reflects it. Hence, decreasing the active layer of the cell [13].

The loss due to parasitic absorption occurs as a result of the absorption of photons by the various layers of the solar cell other than the absorption layer, and those not absorbed by the absorption layer because of its small thickness. Since each layer of the solar cell has its inherent absorption coefficient, a fraction of the incident light is absorbed by these layers, and these absorbed lights cannot partake in the process of generation of electron-hole pairs. Also, because of the small thickness of the absorbing layer, not all the incident light is actually absorbed, leading to losses [13].

2.10.3 The Recombination Loss

This is the type of losses that occurs as a result of recombination of the excess charge carriers. Even after the generation of the electron-hole pairs, they still have to travel to the electrodes where they are to be collected, and its observed that not all the generated charge carriers are collected as some must have recombined either in the bulk, at the interface and/or at the surface of the junction [13].

2.10.4 The Series and Shunt Resistance Loss

The resistance in the bulk, interconnections, contacts, etc. of the semiconductor is called the series resistance. Lattice defects and leakage currents through the edge of the solar cell constitutes the shunt resistance. These losses occur when portions of the photons are transmitted through the solar cell material due to its small thickness [44].

CHAPTER THREE

3.1 SIMULATION PROCEDURE

Modelling and simulation of solar cell devices is a crucial method used in investigating their physical mechanisms without actual fabrication of the device. There are different types of simulation programs developed over the years and applied for research, such as SCAPS-1D (Solar Cells Capacitance Simulator), AMPS-1D (Analysis of Microelectronics and Photonic Structures), PC1D, AFORS-HET, wxAMPS, and many more. These simulation software's can be used to understand the material properties of a solar cell device, by replicating its measurement data. They also help in optimizing the device in a much faster and cheaper way by the modification of the material properties of the device [45]. For the results of the simulation to be calculated in a reasonable amount of time, the programs have to work under certain approximations, assumptions, and limitations.

3.1.1 AMPS 1-D

The Analysis of Microelectronics and Photonic Structures software was developed by Prof. Stephen Fonash, and some fellow workers at the Pennsylvania State University. The software was designed to show how solar cell device physics and device response to light, impressed voltage, and temperature, are controlled by material properties (such as; band gap, affinity, doping, mobilities, defect distributions in the bulk and at interfaces, etc.), and device design/structure.

3.1.1.1 ADVANTAGES OF AMPS 1-D

- I-V characteristics can be generated under illumination and without illumination.
- The QE (SR) for solar cells and photo diodes can be generated under voltage and light bias.
- Can treat devices made up of single crystal, poly-crystalline, or amorphous materials, or any combination.
- Simulation batch processing is allowed
- Provides a friendly user interface, and a flexible plotting program.

3.1.1.2 DISADVANTAGES OF AMPS 1-D

- All information needed for the simulation is required to be entered manually
- Its problem-solving process is slow

3.1.2 PC1D

It is a program developed originally for silicon solar cells, but was later used for simulation of thin-film solar cells. It solves the fully coupled nonlinear equations for the quasi-one-dimensional movement of electrons and holes in crystalline semiconductor devices [46]. The software was developed at the University of New South Wales, Sydney. It has a friendly interface, there is parameter list displayed on screen for each layer and contact in the device, and the parameter values can be changed by clicking on it.

3.1.2.1 ADVANTAGES OF PC1D

- Provides a very easy, and user-friendly interface
- The parameters can be easily modified
- The simulation process is fast.

3.1.2.2 DISADVANTAGES OF PC1D

- It can only be used to model devices with only 5 layers.
- Limited number (200) of time steps in transient excitation mode. This implies that users cannot perform long duration simulations requiring small time steps at the same time [47].

3.1.3 wxAMPS

This solar cell simulation software is an improvement on the AMPS software. It follows the same physical principles of AMPS, but additionally incorporates tunneling currents, improved speed, convergence and visualization. It is designed by the collaboration of two universities, University of Illinois at Urbana Champaign, and Nankai University of China.

3.1.3.1 ADVANTAGES OF wxAMPS

- It has a user-friendly interface, with fast data entry and improved visualization.
- Each device is allowed an unlimited number of layers.

- It is possible to have graded band gaps

3.1.3.2 DISADVANTAGES OF wxAMPS

- It cannot be used in the simulation of non-routine measurements like C-V or C-f.
- Cannot be used to investigate effects of deep interface states on a solar cell [48]

3.1.4 SCAPS 1-D

SCAPS 1-D is a one-dimensional solar cell device simulator developed by Burgelman et al. at the department of Electronics and Information Systems (ELIS) of the University of Gent, Belgium. It is a free, available software, and originally developed for cell structures of the CuInSe₂ and the CdTe [48]. The program allows for up to seven layers to be added for one device, and the physical and electronic properties of each layer can be altered in a separate window. Some advantages and disadvantages of the program are listed below.

3.1.4.1 ADVANTAGES OF SCAPS 1-D

- The simulation process is very fast, and one can include responses of capacitance-voltage, capacitance-frequency, and series resistance.
- Batch calculations are possible.
- Recombination mechanism can be specified
- One can easily grade all parameters

3.1.4.2 DISADVANTAGES OF SCAPS 1-D

- One can only simulate a device with up to seven layers
- When the device is far from ideal and secondary barrier, it may be unstable.
- It can only be used to optimize pn junctions, as it is unstable for np junctions
- Divergence occurs when the variations between different calculation step is not limited [48].

For the course of this work, the SCAPS 1-D simulation software will be used to simulate the behavior of lead-free bismuth perovskite solar cell. The procedure for running a simulation with SCAPS 1-D is illustrated below:

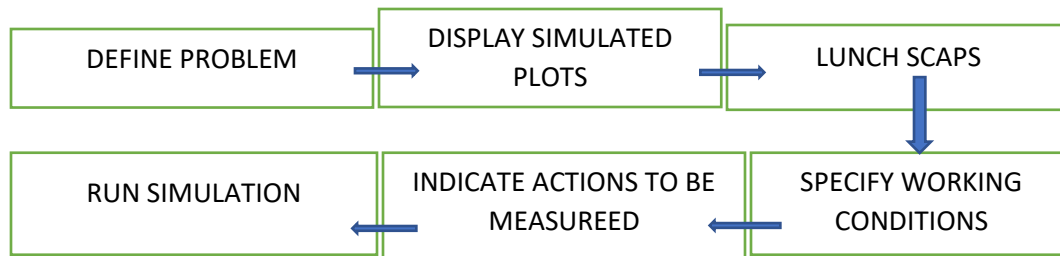


Fig. 10: Flow chart for the operation of the SCAPS 1-D

3.2 SCAPS 1-D INTERFACE

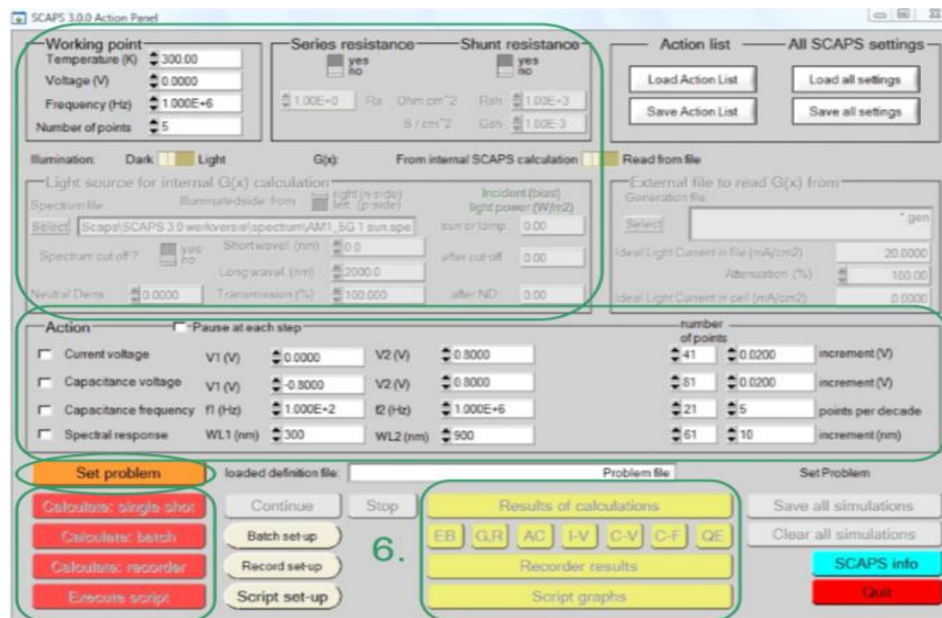


Fig. 11: Panel of the SCAPS 1-D software [49]

When the program is lunched, this window is displayed, and it is divided into different sections, with each section having a significant role.

3.2.1 THE WORKING POINT

This is seen at the top left corner of the displayed action panel, and it identifies clearly and definitely those relevant parameters important to a particular measurement, that are not varied. The working temperature is set at room temperature, 300k. The illumination setting can be dark or light, the illuminated side, and illumination spectrum can be chosen. Although there is a wide range of monochromatic light and spectral choices, the default is a one sun (1000 W/m^2) illumination with the ‘air mass 1.5, global’ spectrum [49].

3.2.2 THE ACTION POINT

It is located just below the working point in the action panel, and this is where the various measurements to be simulated are selected, I-V, C-V, C-f and QE. The orange part labelled “Set Problem” is used to direct the user to the interface for specifying the different layer properties that makes up the solar cell to be simulated. The red icons below the “Set Problem” button is for the commencement of the simulation. It is “Single calculation” when simulation is to be performed on a cell with all parameters kept constant, but “Batch calculation” when properties of the cell layers are varied so as to investigate their effects on the solar cell [49]. The solar cell definition panel is the panel where the different layers that make up the cell is defined. This panel is opened when one clicks on the “Set problem” button in the action panel. This panel helps to create new, or edit solar cell structures. The layer, contacts, and interface properties can be selected by clicking on the assigned box.

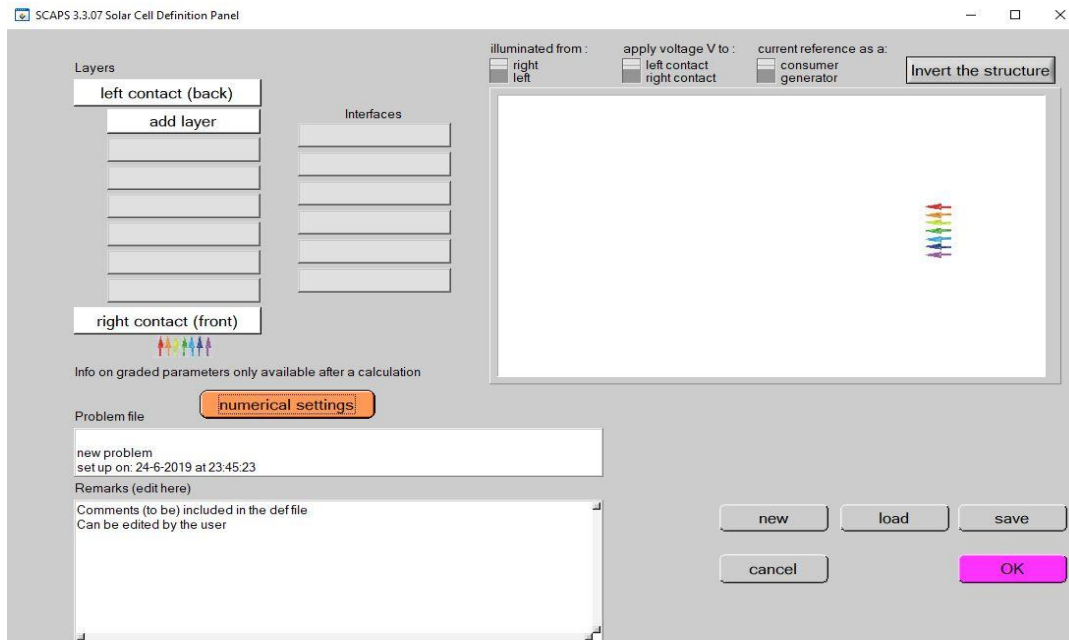


Fig. 12: Solar cell definition panel

3.2.3 LAYER PROPERTIES SPECIFICATION

For a solar cell device to be simulated, all the layer properties must be appropriately defined, as seen in the figure 3.4. These properties include; The layer thickness, band gap (E_g), electron affinity (eV), dielectric permittivity (ϵ), valence, conduction band density of states (N_v and N_c),

electron and hole thermal velocities, charge carriers mobilities (μ_n and μ_p), acceptor and donor dopant concentration, absorption coefficient (α), defect density (N_t), and others [49].

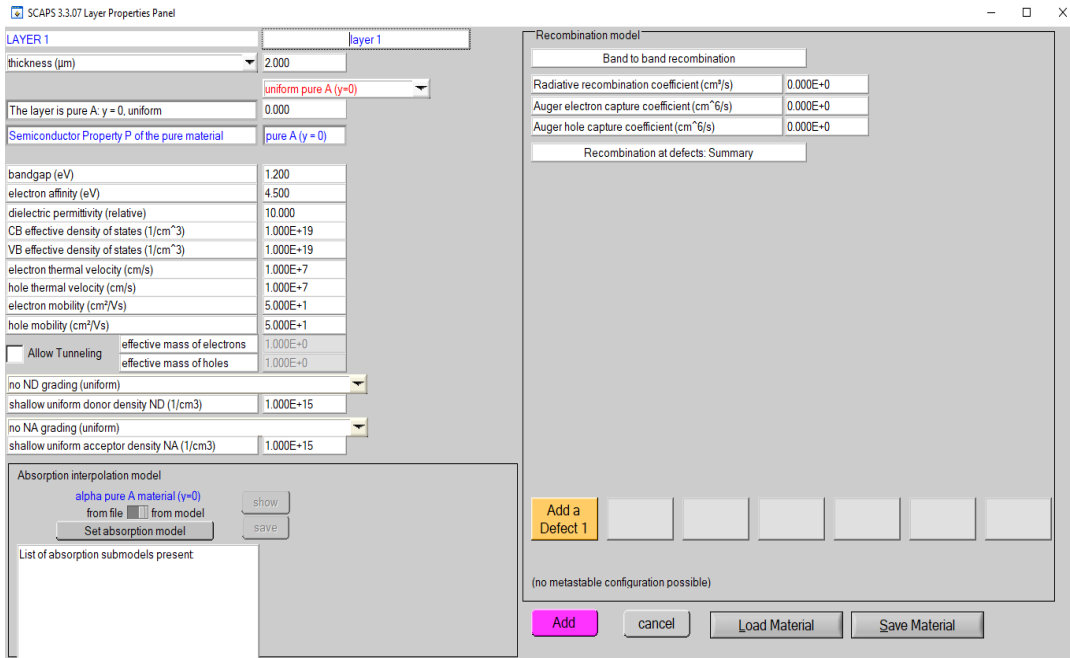


Fig. 13: Layer properties panel, for specifying the properties of the layers that make up the device.

3.2.4 RESULTS OBTAINABLE

After the specification of layer parameters, simulation measurements, and the modelling conditions, one then hits the “single calculation” or “batch calculation” button depending on the calculation to be made. The program shows results of the I-V characteristics, C-F, C-V, energy band diagram, carrier profile, electric field inside the device, generation and recombination of electrons and, lifetime of carriers and quantum efficiency curve [49].

CHAPTER FOUR

4.1 DESIGN AND SIMULATION

The Perovskite solar cell is made up of three main layers; the electron transport layer (ETL), hole transport layer (HTL), and the perovskite layer, which is the absorber layer, sandwiched between the ETL and HTL. Two other important layers that make up the cell are the front and back contact layers. As established earlier, these contacts are responsible for collecting the separated electron-hole pairs, where the front contact collects the electrons, the back contact collects the holes.

4.2 DEVICE ARCHITECTURE

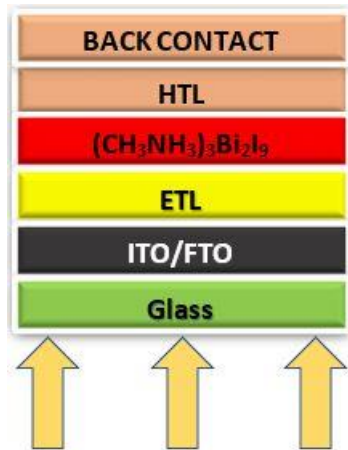


Fig. 14 shows the proposed cell structure with single bismuth-based absorber layer for simulation.

4.3 SIMULATION PARAMETERS

The table below shows the parameters used for the simulation of the solar cell. It includes parameters of the different electron and hole transport layers to be varied. The important parameters were obtained from the following literatures, [49], [50], [51], [52], [53], [54], and [55], whilst others were calculated or estimated. For this work, different cell structures are observed, and comparison is made between the structures having organic hole and electron transport layers, and those having inorganic hole and electron transport layers.

Table 1: Showing the different electrical properties of the proposed solar cell layers for simulation.

Parameters	FTO	ZnO (ETM)	TiO ₂ (ETM)	PCBM (ETM)	P ₃ HT (ETM)	BISMUTH PEROVSKITE	SPIRO- OMETAD (HTM)	Cu ₂ O (HTM)	CuI (HTM)
Thickness (nm)	300	300	300	300	300	100-500	300	300	300
Bandgap (eV)	3.5	3.3	3	2.1	1.8	3.2	3.170	2.1	3.1
Electron affinity (eV)	4	3.9	4	4.1	3.9	4.26	2.050	3.2	2.1
Dielectric permittivity (relative), ϵ_r	9	9	9	9	3	100	3	7.11	6.5
Conduction band effective density of state ($1/\text{cm}^3$)	2.200E+18	1.000E+19	2.200E+18	1.000E+21	1.000E+20	2.0×10^{18}	2.200E+18	2.200E+18	2.500E+20
Valence band effective density of state ($1/\text{cm}^3$)	1.800E+19	1.000E+19	1.900E+19	1.000E+21	1.000E+20	1.8×10^{19}	1.800E+19	1.900E+19	2.500E+20
Electron thermal velocity (cm/s)	1.000E+7	1.000E+7	1.000E+7	1.000E+7	1.000E+7	1.000E+7	1.000E+7	1.000E+7	1.000E+7
Hole thermal velocity (cm/s)	1.000E+7	1.000E+7	1.000E+7	1.000E+7	1.000E+7	1.000E+7	1.000E+7	1.000E+7	1.000E+7
Electron mobility ($\text{cm}^2/\text{V.s}$)	20	50	2	2.000E-3	1.000E-4	4	2.0×10^{-4}	3.4	44
Hole mobility ($\text{cm}^2/\text{V.s}$)	10	5	1	2.000E-4	1.000E-4	2	2.0×10^{-4}	3.4	44
Donor concentration N_D ($1/\text{cm}^3$)	1.000E+18	1.000E+18	1.000E+18	1.000E+21	1.000E+21	1×10^{18}	0	0	0
Acceptor concentration N_A ($1/\text{cm}^3$)	0	0	0	0	0	0	1.0×10^{-4}	1.000E+18	3.000E+18
Defect density N_t ($1/\text{cm}^3$)	1.000E+15	1.000E+15	1.000E+15	1.000E+15	1.000E+15	2.500E+14	1.000E+15	1.000E+15	1.000E+15

4.4 RESULTS AND DISCUSSION

4.4.1 EFFECT OF ABSORBER LAYER THICKNESS

The results displayed below shows the effect of the thickness of the absorber layer on the performances of the different solar cell structures. An optimum absorption layer thickness is necessary for effective absorption of photons for generation of electron-hole pairs. The results displayed below, for all cell structures, shows that the efficiency of the device increases as the absorber thickness increases, up to a maximum point (optimum thickness), where the best efficiency of the device is obtained. The increase in efficiency is as a result of increase in the solar cell characteristics, because a thick absorbing layer will absorb more photons, leading to generation of more electron and hole pairs. The efficiency starts to decrease as the optimum thickness is crossed due to the recombination of the generated electrons and holes as a result of the longer distance the charges have to travel for diffusion.

a) $\text{CuI}/(\text{CH}_3\text{NH}_3)_3\text{Bi}_2\text{I}_9/\text{ZnO}$

Table 2 represents the simulated result for the solar cell characteristics with ZnO and CuI as the electron and hole transport materials respectively, as the thickness of the bismuth layer is varied. The result showed that for a solar cell with this architecture, $\text{CuI}/(\text{CH}_3\text{NH}_3)_3\text{Bi}_2\text{I}_9/\text{ZnO}$, the thickness of the bismuth layer should be within the range of 200-300 nm for optimum performance.

Thickness (μm)	V_{oc} (V)	J_{sc} (mA/cm^2)	FF (%)	Efficiency (%)
1.000e-01	1.2457	4.9077	72.5388	4.4350
2.000e-01	1.2404	6.6162	69.3019	5.6878
3.000e-01	1.2387	6.7258	67.6719	5.6383
4.000e-01	1.2378	6.0118	66.8273	4.9729
5.000e-01	1.2370	5.0215	66.3877	4.1240

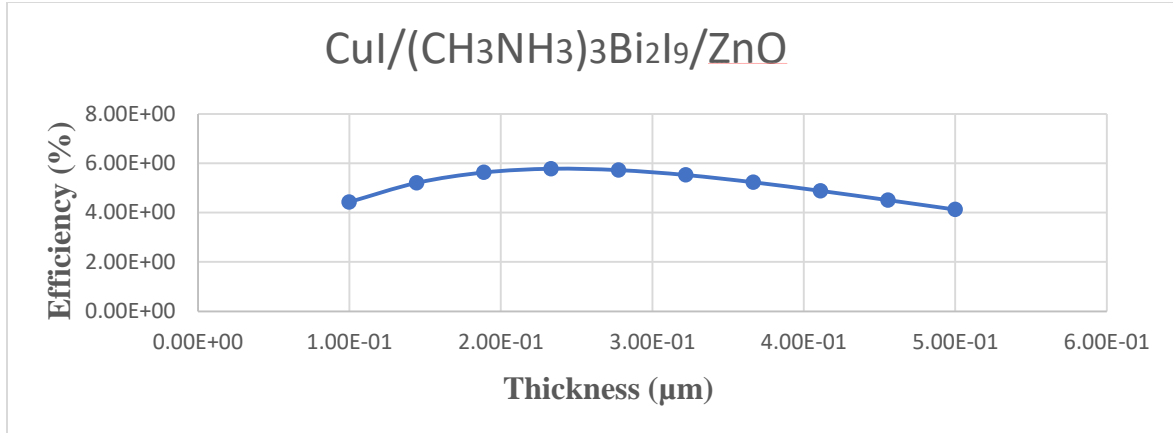


Fig. 15 Graph of the thickness of the bismuth layer vs the efficiency of the solar cell plotted from the simulated results obtained from table 2. This graph clearly shows that the efficiency increases as the thickness of the bismuth layer increases, and gets to a maximum, corresponding to a thickness of about 230 nm, above which any increase in the absorbing layer leads to a decrease in the overall efficiency of the solar cell.

b) $\text{Cu}_2\text{O}/(\text{CH}_3\text{NH}_3)_3\text{Bi}_2\text{I}_9/\text{ZnO}$

Table 3 represents the simulated result for the solar cell characteristics with ZnO and Cu_2O as the electron and hole transport materials respectively, as the thickness of the bismuth layer is varied. The result showed that for a solar cell with this architecture, $\text{Cu}_2\text{O}/(\text{CH}_3\text{NH}_3)_3\text{Bi}_2\text{I}_9/\text{ZnO}$, the thickness of the bismuth layer should be about 200 nm for optimum performance.

Thickness (μm)	V_{oc} (V)	J_{sc} (mA/cm²)	FF (%)	Efficiency (%)
1.000e-01	3.2738	7.5932	23.1802	5.7623
2.000e-01	1.4469	9.1412	46.2114	6.1124
3.000e-01	1.1855	9.8761	47.6564	5.5800
4.000e-01	1.1132	9.4786	43.7889	4.6205
5.000e-01	1.0890	8.0959	40.8141	3.5984

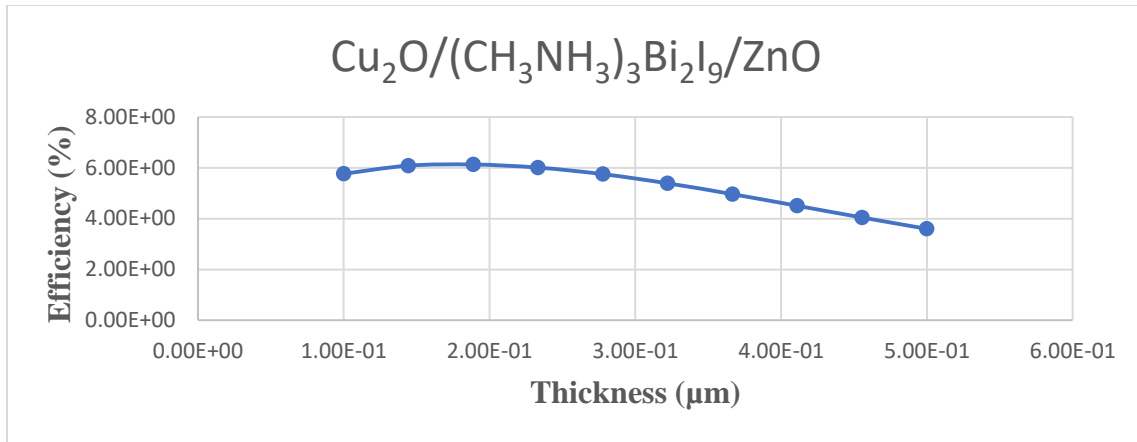


Fig. 16: Present the graph of the thickness of the bismuth layer vs the efficiency of the solar cell plotted from the simulated results obtained from table 3. This graph clearly shows that the efficiency increases as the thickness of the bismuth layer increases, and gets to a maximum, corresponding to a thickness of about 200 nm, above which any increase in the absorbing layer leads to a decrease in the overall efficiency of the solar cell.

c) $\text{Cu}_2\text{O}/(\text{CH}_3\text{NH}_3)_3\text{Bi}_2\text{I}_9/\text{TiO}_2$

Table 3 represents the simulated result for the solar cell characteristics with TiO_2 and Cu_2O as the electron and hole transport materials respectively, as the thickness of the bismuth layer is varied. The result showed that for a solar cell with this architecture, $\text{Cu}_2\text{O}/(\text{CH}_3\text{NH}_3)_3\text{Bi}_2\text{I}_9/\text{TiO}_2$, the thickness of the bismuth layer should be about 200 nm for optimum performance.

Thickness (μm)	V_{oc} (V)	J_{sc} (mA/cm ²)	FF (%)	Efficiency (%)
1.000e-01	3.3172	7.4086	22.8874	5.6249
2.000e-01	1.449624	8.9874	46.2630	6.0273
3.000e-01	1.1914	9.7487	47.5865	5.5272
4.000e-01	1.1170	9.3854	43.7726	4.5892
5.000e-01	1.0894	8.0352	40.9043	3.5806

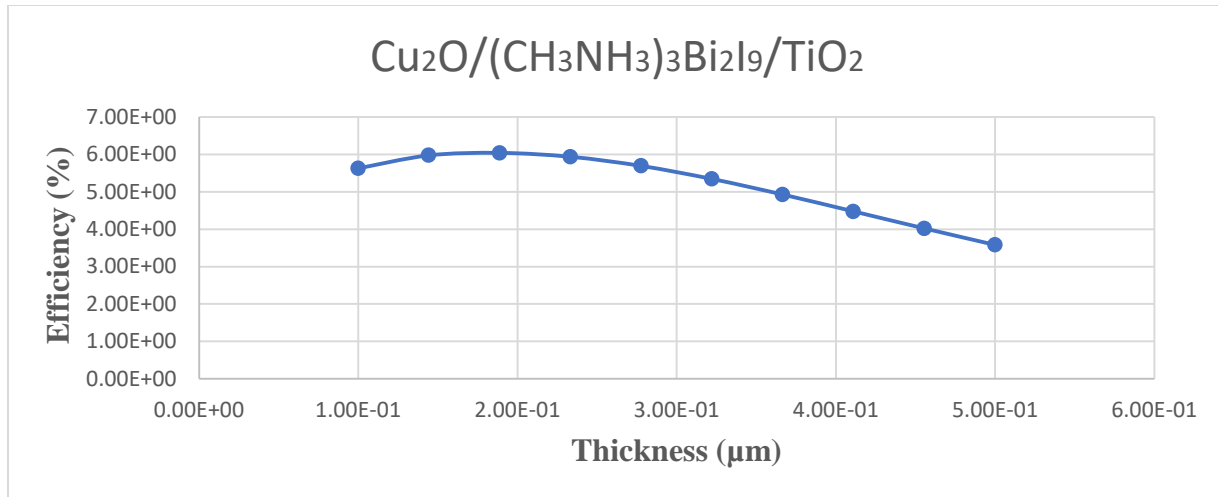


Fig. 17 represents the graph of the thickness of the bismuth layer vs the efficiency of the solar cell plotted from the simulated results obtained from table 4. This graph clearly shows that the efficiency increases as the thickness of the bismuth layer increases, and gets to a maximum, corresponding to a thickness of about 200nm, above which any increase in the absorbing layer leads to a decrease in the overall efficiency of the solar cell.

d) CuI/(CH₃NH₃)₃Bi₂I₉/TiO₂

Table 4 represents the simulated result for the solar cell characteristics with TiO₂ and CuI as the electron and hole transport materials respectively, as the thickness of the bismuth layer is varied. The result showed that for a solar cell with this architecture, CuI/(CH₃NH₃)₃Bi₂I₉/TiO₂, the thickness of the bismuth layer should be about 200nm for optimum performance.

Thickness (μm)	V_{oc} (V)	J_{sc} (mA/cm²)	FF (%)	Efficiency (%)
1.000e-01	1.2462	4.6513	71.2243	4.1286
2.000e-01	1.2411	6.0305	67.9872	5.0886
3.000e-01	1.2394	5.7325	66.5484	4.7283
4.000e-01	1.2396	4.7834	65.8976	3.9077
5.000e-01	1.2393	3.7524	65.4707	3.0448

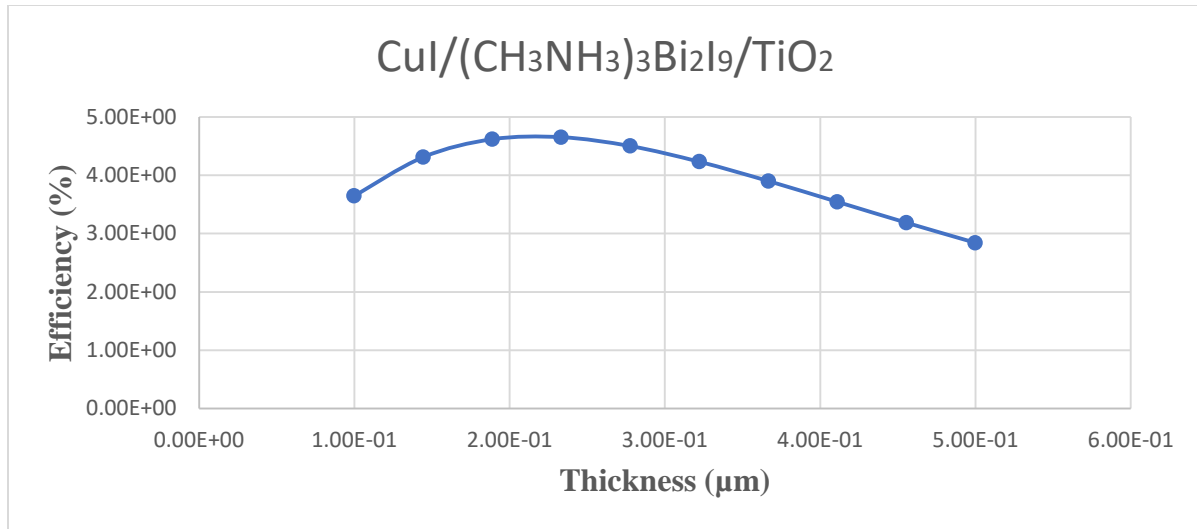


Fig. 18: represents the graph of the thickness of the bismuth layer vs the efficiency of the solar cell plotted from the simulated results obtained from table 5. This graph clearly shows that the efficiency increases as the thickness of the bismuth layer increases, and gets to a maximum, corresponding to a thickness of about 200-230 nm, above which any increase in the absorbing layer leads to a decrease in the overall efficiency of the solar cell.

e) SPIRO-OMETAD/(CH₃NH₃)₃Bi₂I₉/PCBM

Table 5 represents the simulated result for the solar cell characteristics with PCBM and SPIRO-OMeTAD as the electron and hole transport materials respectively, as the thickness of the bismuth layer is varied. The result showed that for a solar cell with this architecture, SPIRO-OMETAD/(CH₃NH₃)₃Bi₂I₉/PCBM, the thickness of the bismuth layer should be about 300nm for optimum performance.

Thickness (μm)	V_{oc} (V)	J_{sc} (mA/cm²)	FF (%)	Efficiency (%)
1.000e-01	1.2542	4.0863	74.1771	3.8018
2.000e-01	1.2455	6.1375	71.0678	5.4327
3.000e-01	1.2429	6.7399	69.3694	5.8112
4.000e-01	1.2417	6.4659	68.4177	5.4932
5.000e-01	1.2410	5.7637	67.8953	4.8566

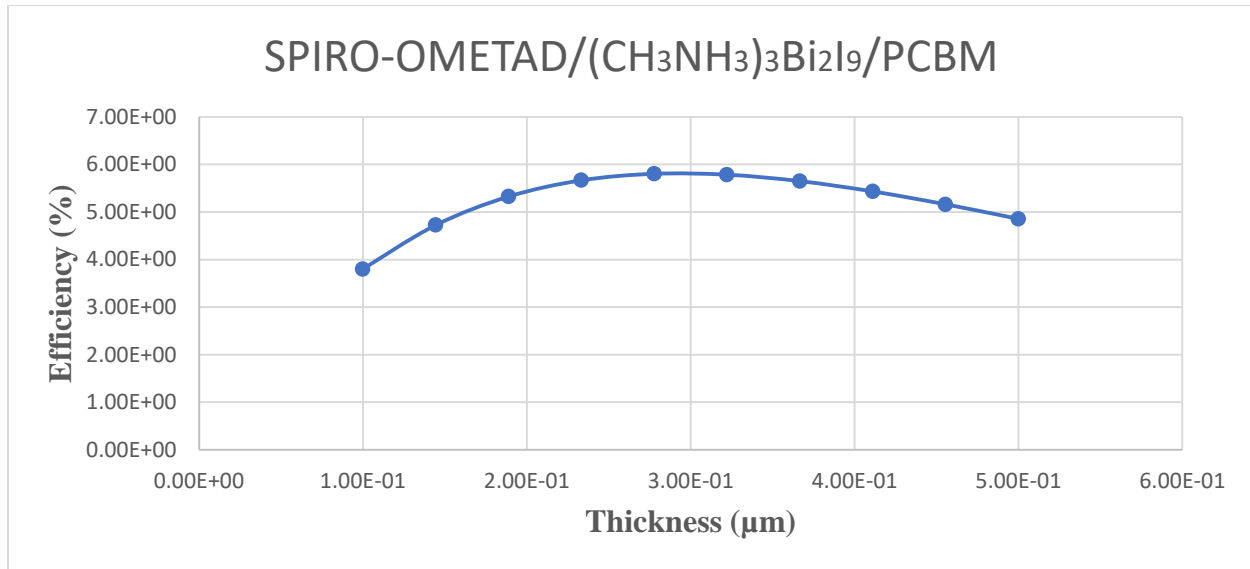


Fig. 19 represents the graph of the thickness of the bismuth layer vs the efficiency of the solar cell plotted from the simulated results obtained from table 6. This graph clearly shows that the efficiency increases as the thickness of the bismuth layer increases, and gets to a maximum, corresponding to a thickness of about 300 nm, above which any increase in the absorbing layer leads to a decrease in the overall efficiency of the solar cell.

f) SPIRO-OMETAD/(CH₃NH₃)₃Bi₂I₉/P₃HT

Table 6 represents the simulated result for the solar cell characteristics with P₃HT and SPIRO-OMeTAD as the electron and hole transport materials respectively, as the thickness of the bismuth layer is varied. The result showed that for a solar cell with this architecture, SPIRO-OMETAD/(CH₃NH₃)₃Bi₂I₉/P₃HT, the thickness of the bismuth layer should be about 300 nm for optimum performance.

Thickness (μm)	V _{oc} (V)	J _{sc} (mA/cm ²)	FF (%)	Efficiency (%)
1.000e-01	1.2507	4.0250	72.7949	3.6651
2.000e-01	1.2446	5.9749	70.4103	5.2363
3.000e-01	1.2425	6.5135	69.0279	5.5868
4.000e-01	1.2415	6.2262	68.2341	5.2747
5.000e-01	1.2409	5.5435	67.7953	4.6639

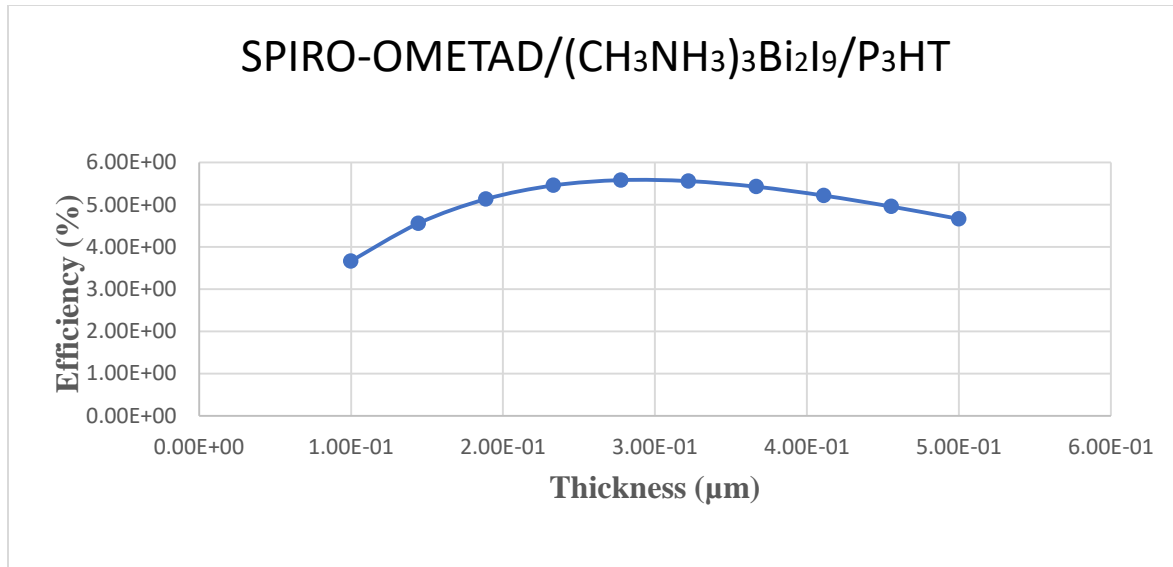


Fig. 20 represents the graph of the thickness of the bismuth layer vs the efficiency of the solar cell plotted from the simulated results obtained from table 7. This graph clearly shows that the efficiency increases as the thickness of the bismuth layer increases, and gets to a maximum, corresponding to a thickness of about 300 nm, above which any increase in the absorbing layer leads to a decrease in the overall efficiency of the solar cell.

4.4.2 EFFECT OF ORGANIC AND INORGANIC TRANSPORT LAYERS

Here, the transport materials were varied, with the thickness of the absorbing layer kept constant at 250 nm, to understand its influence on the efficiency of the device. From the table below, it is clearly seen that the efficiency of the perovskite solar cell largely depends on the type of charge transport materials used, and the method of combination. Different combinations gave different values of efficiency, the minimum value of efficiency (2.32 %), was realized with the $\text{CuI}/(\text{CH}_3\text{NH}_3)_3\text{Bi}_2\text{I}_9/\text{TiO}_2$ device structure, whilst the device, $\text{Cu}_2\text{O}/(\text{CH}_3\text{NH}_3)_3\text{Bi}_2\text{I}_9/\text{ZnO}$, had the best performance with an efficiency of 6.01 %. the device with the best performance is made with inorganic transport materials, and with higher stability than devices with organic transport materials under atmospheric conditions.

Table 7 shows the simulated results for the cell characteristics of the different solar cell architectures, that is, those with inorganic and organic transport materials (electron and hole layers). The architecture with inorganic transport materials had the best performance with an efficiency of 6.01 %.

PEROVSKITE STRUCTURE	V_{oc} (V)	J_{sc} (mA/cm²)	FF (%)	EFFICIENCY (%)
CuI/(CH ₃ NH ₃) ₃ Bi ₂ I ₉ /ZnO	1.2398	6.7887	68.64	5.78
Cu ₂ O/(CH ₃ NH ₃) ₃ Bi ₂ I ₉ /ZnO	1.3336	9.4854	47.50	6.01
Cu ₂ O/(CH ₃ NH ₃) ₃ Bi ₂ I ₉ /TiO ₂	1.3360	9.3397	47.57	5.94
CuI/(CH ₃ NH ₃) ₃ Bi ₂ I ₉ /TiO ₂	1.2390	2.8539	65.66	2.32
SPIRO-OMETAD/(CH ₃ NH ₃) ₃ Bi ₂ I ₉ /PCBM	1.2444	6.4669	70.40	5.66
SPIRO-OMETAD/(CH ₃ NH ₃) ₃ Bi ₂ I ₉ /P ₃ HT	1.2438	6.2774	69.87	5.46

4.4.3 EFFECT OF TEMPERATURE

The graphs below clearly show the effects of temperature on the different solar cell structures. The temperature was varied from 295 K to 320 K. It can be seen that the temperature varies with the different cell device type. That is to say that the effect of temperature on the characteristics of a device also depends on the transport materials. Generally, the temperature at which the device is exposed to affects its performance.

a) CuI/(CH₃NH₃)₃Bi₂I₉/ZnO

Table 8 represents the simulated result for the solar cell characteristics with ZnO and CuI as the electron and hole transport materials respectively, with variation in the temperature of the illumination light. The table shows that changes in the temperature of the illuminated light results in changes in efficiency of the solar cell.

Temperature (K)	V_{oc} (V)	J_{sc} (mA/cm²)	FF (%)	Efficiency (%)
2.95E+02	1.2387	6.7666	68.9586	5.78E+00
3.00E+02	1.2397	6.7887	68.6424	5.77E+00

3.05E+02	1.2403	6.8103	68.3418	5.78E+00
3.10E+02	1.2407	6.8312	68.0543	5.77E+00
3.15E+02	1.2407	6.8516	67.7882	5.76E+00
3.20E+02	1.2401	6.8715	67.5567	5.76E+00

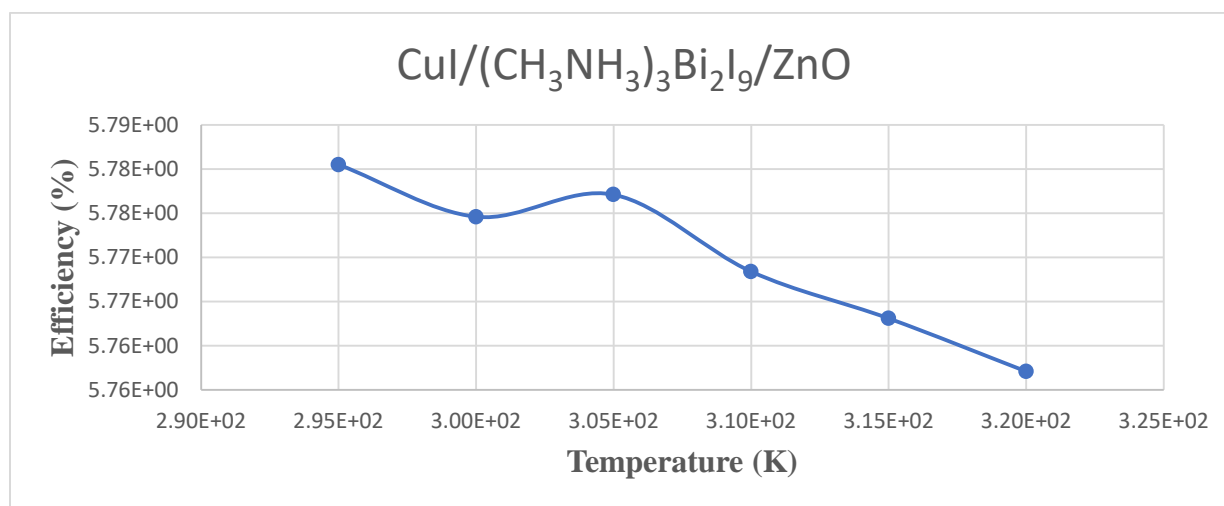


Fig. 21 represents the graph of temperature vs efficiency obtained from the simulated result in table 9. The best performance for this solar cell architecture is gotten when the temperature of illumination is at 295 k and as the temperature is increased to 320 k, the efficiency decreased slightly.

b) $\text{Cu}_2\text{O}/(\text{CH}_3\text{NH}_3)_3\text{Bi}_2\text{I}_9/\text{ZnO}$

Table 9 represents the simulated result for the solar cell characteristics with ZnO and Cu_2O as the electron and hole transport materials respectively, with variation in the temperature of the illumination light. The table shows that changes in the temperature of the illuminated light results in changes in efficiency of the solar cell.

Temperature (K)	V_{oc} (V)	J_{sc} (mA/cm ²)	FF (%)	Efficiency (%)
2.95E+02	1.363074	9.480444	46.8396	6.05E+00

3.00E+02	1.317742	9.48548	48.0729	6.01E+00
3.05E+02	1.276224	9.490452	49.2431	5.96E+00
3.10E+02	1.241673	9.495269	50.2043	5.92E+00
3.15E+02	1.204784	9.499933	51.3195	5.87E+00
3.20E+02	1.174217	9.504423	52.2276	5.83E+00

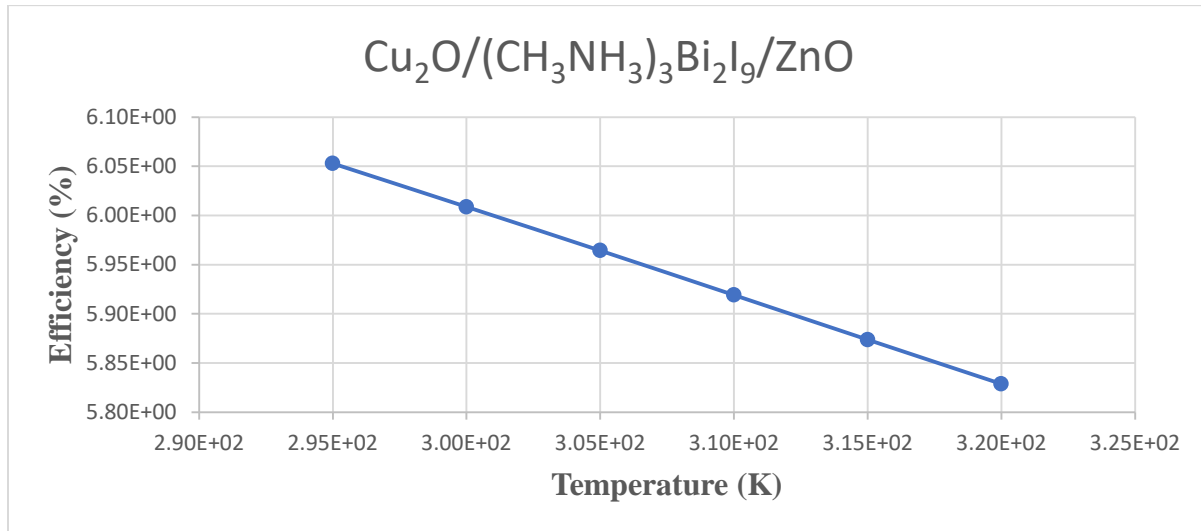


Fig. 22 represents the graph of temperature vs efficiency obtained from the simulated result in table 10. The best performance for this solar cell architecture is gotten when the temperature of illumination is at 295 k and as the temperature is increased to 320 k, the efficiency decreases.

c) $\text{Cu}_2\text{O}/(\text{CH}_3\text{NH}_3)_3\text{Bi}_2\text{I}_9/\text{TiO}_2$

Table 10 represents the simulated result for the solar cell characteristics with TiO_2 and Cu_2O as the electron and hole transport materials respectively, with variation in the temperature of the illumination light. The table shows that changes in the temperature of the illuminated light results in changes in efficiency of the solar cell.

Temperature (K)	V_{oc} (V)	J_{sc} (mA/cm^2)	FF (%)	Efficiency (%)
2.95E+02	1.3676	9.334	46.8383	5.98E+00
3.00E+02	1.3229	9.3397	48.0406	5.94E+00

3.05E+02	1.2791	9.3447	49.2882	5.89E+00
3.10E+02	1.2404	9.3495	50.4106	5.85E+00
3.15E+02	1.2050	9.3543	51.4616	5.80E+00
3.20E+02	1.1746	9.3589	52.3568	5.76E+00

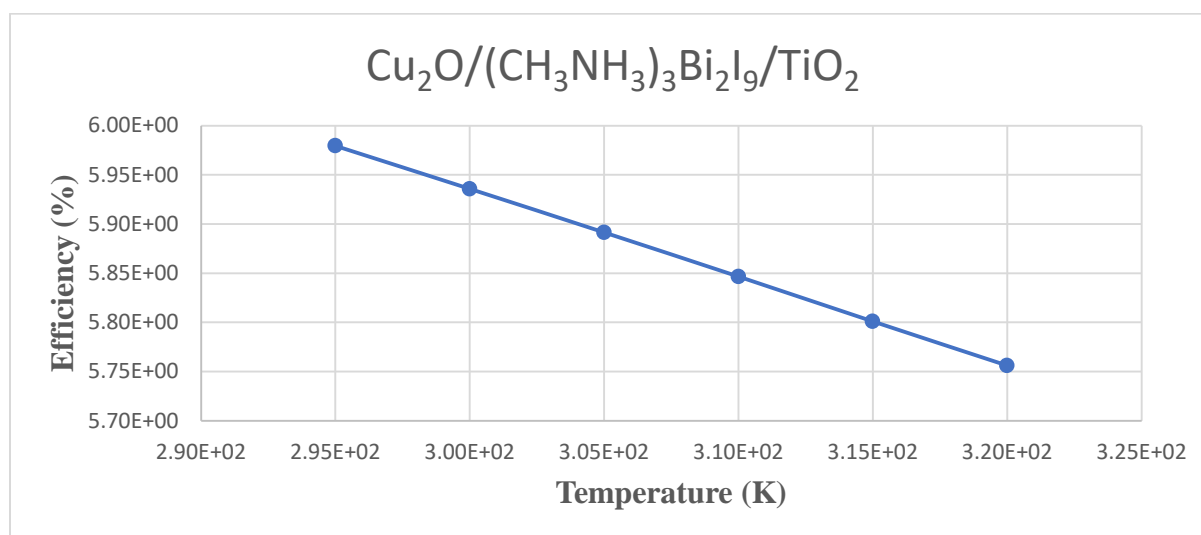


Fig. 23 represents the graph of temperature vs efficiency obtained from the simulated result in table 11. The best performance for this solar cell architecture is gotten when the temperature of illumination is at 295 k and as the temperature is increased to 320 k, the efficiency decreases.

d) CuI/(CH₃NH₃)₃Bi₂I₉/TiO₂

Table 11 represents the simulated result for the solar cell characteristics with TiO₂ and CuI as the electron and hole transport materials respectively, with variation in the temperature of the illumination light. The table shows that changes in the temperature of the illuminated light results in changes in efficiency of the solar cell.

Temperature (K)	V_{oc} (V)	J_{sc} (mA/cm²)	FF (%)	Efficiency (%)
2.95E+02	1.2386	2.8171	66.0111	2.30E+00
3.00E+02	1.2390	2.8539	65.6606	2.32E+00
3.05E+02	1.2390	2.8904	64.9765	2.33E+00

3.10E+02	1.2363	2.9267	64.8776	2.35E+00
3.15E+02	1.2350	2.9627	64.6726	2.37E+00
3.20E+02	1.2322	2.9984	64.799	2.39E+00

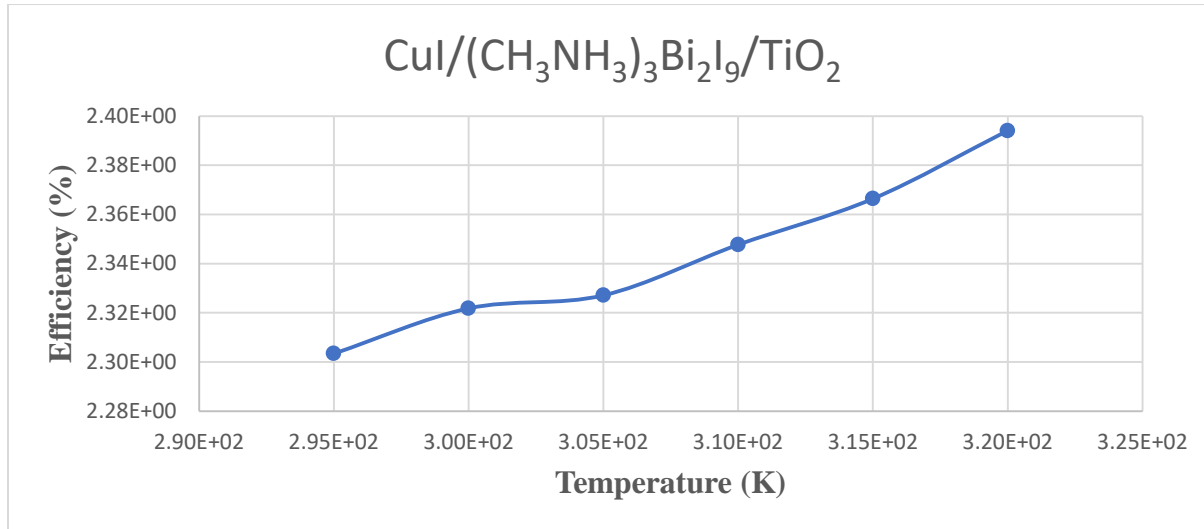


Fig. 24 represents the graph of temperature vs efficiency obtained from the simulated result in table 12. As the temperature increases from 295 k to 320 k, the efficiency of the solar cell increases also. The best performance for this solar cell architecture was gotten when the temperature of illumination is at 320 k.

e) SPIRO-OMETAD/(CH₃NH₃)₃Bi₂I₉/PCBM

Table 12 represents the simulated result for the solar cell characteristics with PCBM and SPIRO-OMETAD as the electron and hole transport materials respectively, with variation in the temperature of the illumination light. The table shows that changes in the temperature of the illuminated light results in changes in efficiency of the solar cell.

Temperature (K)	V_{oc} (V)	J_{sc} (mA/cm²)	FF (%)	Efficiency (%)
2.95E+02	1.2435	6.4540	70.7222	5.68E+00

3.00E+02	1.2443	6.4669	70.395	5.67E+00
3.05E+02	1.2451	6.4795	70.0723	5.65E+00
3.10E+02	1.2457	6.4916	69.7578	5.64E+00
3.15E+02	1.2461	6.5035	69.4551	5.63E+00
3.20E+02	1.2462	6.5149	69.1722	5.62E+00

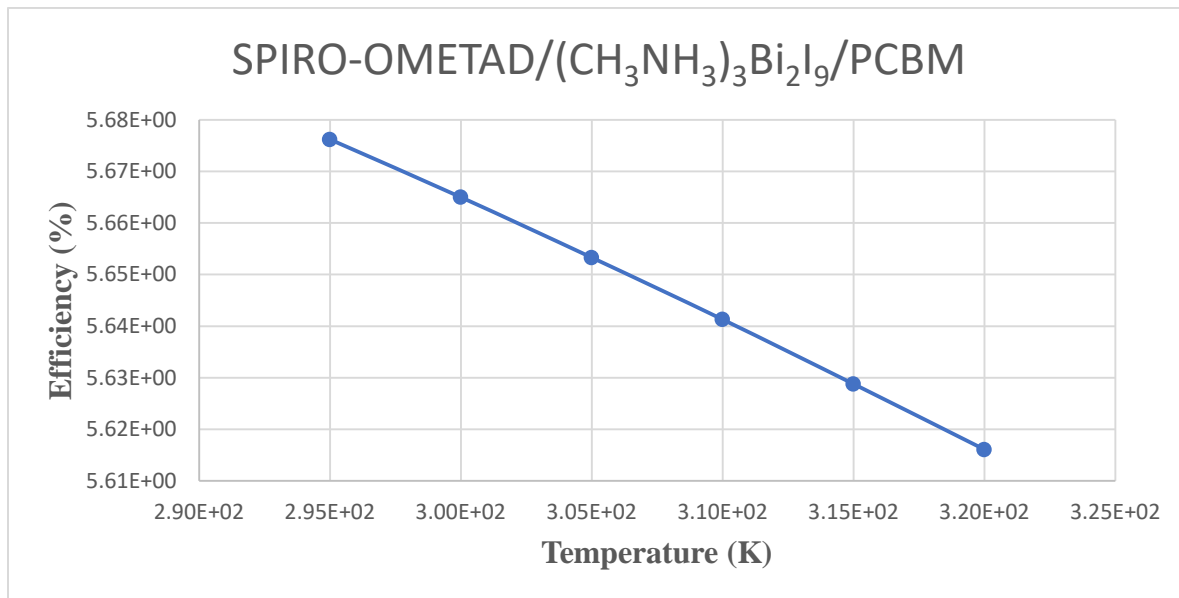


Fig. 25 represents the graph of temperature vs efficiency obtained from the simulated result in table 13. The best performance for this solar cell architecture is gotten when the temperature of illumination is at 295 k and as the temperature is increased to 320 k, the efficiency decreases.

f) SPIRO-OMETAD/(CH₃NH₃)₃Bi₂I₉/P₃HT

Table 13 represents the simulated result for the solar cell characteristics with P₃HT and SPIRO-OMETAD as the electron and hole transport materials respectively, with variation in the temperature of the illumination light. The table shows that changes in the temperature of the illuminated light results in changes in efficiency of the solar cell.

Temperature (K)	V _{oc} (V)	J _{sc} (mA/cm ²)	FF (%)	Efficiency (%)
2.95E+02	1.2429	6.2401	70.1506	5.44E+00
3.00E+02	1.2437	6.2774	69.8696	5.46E+00
3.05E+02	1.2445	6.3138	69.595	5.47E+00
3.10E+02	1.2451	6.3485	69.3281	5.48E+00
3.15E+02	1.2462	6.3810	69.0366	5.49E+00
3.20E+02	1.2452	6.4110	68.8601	5.50E+00

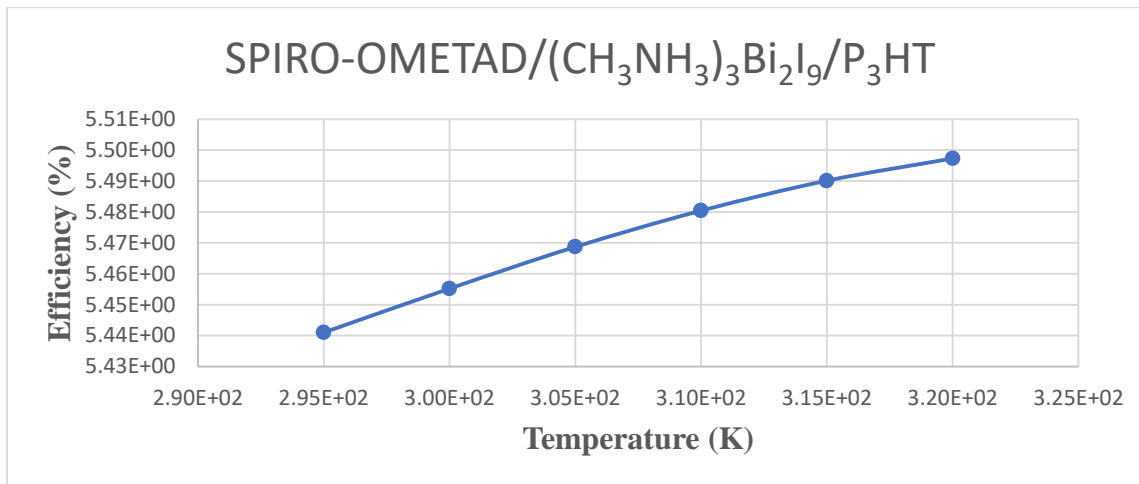


Fig. 26 represents the graph of temperature vs efficiency obtained from the simulated result in table 14. As the temperature increases from 295 k to 320 k, the efficiency of the solar cell increases also. The best performance for this solar cell architecture was gotten when the temperature of illumination is at 320 k.

CHAPTER FIVE

5.1 CONCLUSION

In this work, cell devices using inorganic electron and hole transport materials, and those with organic electron and hole transport materials were simulated. The organic ETLs are P3HT and PCBM, and the HTL is Spiro-Ometad, whilst the inorganic ETLs are ZnO and TiO₂, the HTLs are CuI, Cu₂O. For each device structure, the thickness of the bismuth based absorbing layer was varied from 100 nm to 500 nm. The best performance was obtained from the device with inorganic electron and hole transport materials, Cu₂O/(CH₃NH₃)₃Bi₂I₉/ZnO, with V_{oc} of 1.4 V, J_{sc} of 9.1 mA/cm², FF of 46.2 %, and efficiency of 6.1 %, at a thickness of 200 nm. The best performing device with organic transport materials, Spiro-Ometad/(CH₃NH₃)₃Bi₂I₉/PCBM, with V_{oc} of 1.2 V, J_{sc} of 6.7 mA/cm², FF of 69.3 %, and efficiency of 5.8 %, at a thickness of 300 nm. Hence, the device with inorganic transport materials has shown great promise as it delivers a higher efficiency with less absorber material quantity than the device with organic transport materials. The temperature was also varied from 295 k to 320 k, and it was seen that the different cell structures had different responses as the temperature increases. This is due to the influence of the different charge transport materials on the cell characteristics.

5.2 RECOMMENDATION

This simulation was carried out for a few organic and inorganic transport materials, hence, other transport materials can be investigated, like PEDOT:PSS, NiO, CuSCN, and a bismuth based cell having a combination of organic and inorganic transport material should also be investigated. Also, an experimental work can be done to validate the results from the simulation.

REFERENCES

- [1] J. J. M. Halls, C. A. Walsh, N. C. Greenham, E. A. Marseglia, R. H. Friend and S. C. & H. A. B. Moratti, "Efficient photodiodes from interpenetrating polymer networks," *Nature*, p. 498 – 500, 1995.
- [2] N. Kour and R. Mehra, "Recent Advances in Photovoltaic Technology based on Perovskite Solar Cell- A Review," *International Research Journal of Engineering and Technology (IRJET)*, pp. 1284-1296, 2017.
- [3] F. M. Smits, "History of Silicon Solar Cells," *IEEE Transactions on electron devices*, pp. 640-643, 1976.
- [4] "Perovskites and Perovskite Solar Cells: An Introduction," Sheffield.
- [5] H.-J. Du, W.-C. Wang and J.-Z. Zhu, "Device simulation of lead-free CH₃NH₃SnI₃ perovskite solar cells with high efficiency," *Chin.Phys.B*, pp. 108802 (1-8), 2016.
- [6] M. Lazemi, S. Asgharizadehb and S. Belluccia, "A Computational Approach to Interface Engineering of Lead-Free CH₃NH₃SnI₃ Highly-Efficient Perovskite Solar Cells," *Phys. Chem. Chem. Phys.*, pp. 1-10, 2018.
- [7] A. Kulkarni, T. Singh, M. Ikegami and T. Miyasaka, "Photovoltaic enhancement of bismuth halide hybrid perovskite by N-methyl pyrrolidone-assisted morphology conversion," *The Royal Society of Chemistry*, vol. 7, p. 9456–9460, 2017.
- [8] W. Miaoqiang Lyu¹, G. Liu and L. Wang, "Organic–inorganic bismuth (III)-based material: A leadfree, air-stable and solution-processable light-absorber beyond organolead perovskites," *Springer*, pp. 1-11, 2015.
- [9] N. S. S. Exploration, "A. NASA solar system exploration," [Online]. Available: <https://solarsystem.nasa.gov/solar-system/sun/overview/>. [Accessed 17 May 2019].
- [10] S. A. T. Environmental Decision Making, "Environmental Decision Making, Science, and Technology," [Online]. Available: <http://environ.andrew.cmu.edu/m3/s2/02sun.shtml>. [Accessed 17 May 2019].
- [11] "PVE ducation," [Online]. Available: <https://www.pveducation.org/pvcdrom/properties-of-sunlight/atmospheric-effects>. [Accessed 17 May 2019].
- [12] "Science Daily," [Online]. Available: https://www.sciencedaily.com/terms/solar_cell.htm. [Accessed 17 MAY 2019].
- [13] K. Jäger, O. Isabella, A. H. Smets, R. A. v. Swaaij and M. Zeman, *Solar Energy Fundamentals, Technology, and Systems*, Delft, Netherlands, 2014.
- [14] O. Simya¹, P. Radhakrishnan and A. Ashok, "Engineered Nanomaterials for Energy Applicati," in *Handbook of Nanomaterials for Industrial Applications.*, india, Elsevier, 2018.

- [15] K. Ranabhat, L. Patrikeev, A. A. Revina, K. Andrianov, V. Lapshinsky and E. Sofronova, "An Introduction To Solar Cell Technology," *Journal of Applied Engineering Science* , vol. 14, no. 4, pp. 481-491, 2016.
- [16] M. T. Kibria, A. Ahammed, S. M. Sony, F. Hossain and Shams-UI-Islam, "A Review: Comparative studies on different generation solar cells technology," in *International Conference on Environmental Aspects of Bangladesh* , Bangladesh , 2014.
- [17] "Top-Alternative-Energy-Solutions," [Online]. Available: <http://www.top-alternative-energy-sources.com/solar-cells.html>. [Accessed 21 MAY 2019].
- [18] H. J. Snaith, "Perovskites: The Emergence of a New Era for Low-Cost, HighEfficiency Solar Cells," *The Journal of Physical Chemistry Letters*, no. 4, pp. 3623-3630, 2013.
- [19] R. J. d. Tilley, *Perovskites: Structure–Property Relationships*, West Sussex: John Wiley & Sons, Ltd, 2016 .
- [20] G. E. Eperon, "Active Layer Control for High Efficiency Perovskite Solar Cells," Oxford, 2015.
- [21] C. Zuo, H. J. Bolink, H. Han, J. Huang, D. Cahen and a. L. Ding, "Advances in Perovskite Solar Cells," *Advanced Science*, pp. 1-16, 2016.
- [22] P. Kajal, K. Ghosh and S. Powar, "Manufacturing Techniques of Perovskite Solar Cells," 2018.
- [23] N. Marinova, S. Valero and J. L. Delgado, "Organic and Perovskite Solar Cells: Working Principles, Materials and Interfaces," *Elsevier*, vol. 488, p. 373–389, 2017.
- [24] R. Sheng, A. Ho-Baillie, S. Huang, S. Chen, X. Wen and X. Hao., "Methylammonium Lead Bromide Perovskite-Based Solar Cells by Vapor-Assisted Deposition," *Journal of Physical Chemistry*, no. 119, p. 3545–3549, 2015.
- [25] N. K. Noel, S. D. Stranks, A. Abate, C. Wehrenfennig, S. Guarnera, A.-A. Haghighirad, A. Sadhanala, G. E. Eperon, S. K. Pathak, M. B. Johnston, A. Petrozza, L. M. Herz and H. j. snaith, "Lead-free organic–inorganic tin halide perovskites for photovoltaic applications," *The Royal Society of Chemistry* , vol. 7, pp. 3061-3068, 2014.
- [26] M.-C. Jung, S. R. Raga and Y. Qi, "Properties and solar cell applications of Pb-free perovskite films formed by vapor deposition," *The Royal Society of Chemistry* , pp. 1-8, 2013.
- [27] P. C. Harikesh, H. K. Mulmudi, B. Ghosh, T. W. Goh, Y. T. Teng, K. Thirumal, M. Lockrey, K. Weber, T. M. Koh, S. Li, S. Mhaisalkar and N. Mathews, "Rb as an Alternative Cation for Templating Inorganic Lead-Free Perovskites for Solution Processed Photovoltaics," *Chemistry of Materials*, pp. 7496-7504, 2016.
- [28] P. Kajal, K. Ghosh and S. Powar, "Manufacturing Techniques of Perovskite Solar Cells," pp. 341-364, 2017.
- [29] Z. Shi and A. H. Jayatissa, "Perovskites-Based Solar Cells: A Review of Recent Progress, Materials and Processing Methods," *Materials* , pp. 1-34, 2018.

- [30] M. Habibi, A. Rahimzadeh, I. Bennouna and M. Eslamian, "Defect-Free Large-Area (25 cm²) Light Absorbing Perovskite Thin Films Made by Spray Coating," *coatings*, pp. 1-15, 2017.
- [31] "TEL nanotec museum," [Online]. Available: <https://www.tel.com/museum/exhibition/principle/semiconductor.html>. [Accessed 25 MAY 2019].
- [32] S. Fonash, *Solar Cell Device Physics*, Oxford: Elsevier, 2010.
- [33] D.-k. Seo and R. Hoffmann, "Direct and indirect band gap types in one-dimensional conjugated or stacked organic materials," *Theoretical Chemistry Account*, vol. 102, pp. 23-32, 1999.
- [34] U. K. MISHRA and J. SINGH, *Semiconductor Device Physics and Design*, AA Dordrecht: Springer, 2008.
- [35] D. A. Neamen, *Semiconductor Physics and Devices*, New York: McGraw-Hill, 2012.
- [36] R. Santbergen and R. V. zolingen, "The absorption factor of crystalline silicon PV cells: A numerical and experimental study," *Science Direct*, pp. 1-13, 2007.
- [37] R. J. B. Balaguru and B. G. Jeyaprakash, "Energy Bands, Basics of Transports and Optical Processes in Semiconductors," NPTEL – Electrical & Electronics Engineering – Semiconductor Nanodevices.
- [38] S. Kasap, *Principles of electronic materials and devices*, New York: McGraw-Hill, 2006.
- [39] R. E. Hummel, *Electronic Properties of Materials*, New York: Springer, 2001.
- [40] J.-p. colinge and C. A. colinge, *Physics of Semiconductor Devices*, Dordrecht: Kluwer Academic, 2002.
- [41] A. Reinders, P. Verlinden and W. v. Sark, *Photovoltaic Solar EnErgy*, West Sussex: John Wiley & Sons, Ltd, 2017.
- [42] S. S. Li, *Semiconductor Physical Electronics*, NewYork: Springer, 2006.
- [43] T. Soga, *Nanostructured Materials for Solar Energy Conversion*, Elsevier, 2001.
- [44] R. Knecht, "Basics of Photovoltaics," *Renewable Energy Online*, 2017.
- [45] "University of North South Wales, sydney," [Online]. Available: <https://www.engineering.unsw.edu.au/energy-engineering/research/software-data-links/pc1d-software-for-modelling-a-solar-cell>. [Accessed 28 June 2019].
- [46] K. Wang and I. Perez-Wurfl, "A method to overcome the time step limitation of PC1D in transient excitation mode," *Elsevier*, no. 55, pp. 155-160, 2014.
- [47] M. A. Sayeed and I. Salem, "Design and Simulation of Efficient Perovskite Solar Cells," Bangladash, 2017.
- [48] M. Burgelman, K. Decock, A. Niemegeers, J. Verschraegen and S. Degrave, "SCAPS MANUAL," Gent, 2018.

- [49] G. Casas, M. Cappelletti, A. Cédola, B. M. Soucase and E. P. Blancá, "Analysis of the power conversion efficiency of perovskite solar cells with different materials as Hole-Transport Layer by numerical simulations," *Superlattices and Microstructures*, 2017.
- [50] S. Bansal and P. Aryal, "Evaluation of New Materials for Electron and Hole Transport Layers in Perovskite-Based Solar Cells Through SCAPS-1D Simulations," *IEEE*, pp. 747-750, 2016.
- [51] U. Mandadapu, D. S. V. Vedanayakam and D. K. Thyagarajan, "Numerical Simulation of $\text{CH}_3\text{NH}_3\text{PbI}_3\text{-XCl}_x$ Perovskite solar cell using SCAPS-1D," *International Journal of Engineering Science Invention*, pp. 40-45, 2017.
- [52] F. Sadeghia and M. Neghabi, "Optimization of Structure of Solar Cells Based on Lead Perovskites ($\text{CH}_3\text{NH}_3\text{PbX}_3$, X: I, Br)," *Journal of Solar Energy Research (JSER)*, vol. 2, no. 4, pp. 315-321, 2017.
- [53] E. Karimi and S. M. B. Ghorashi, "Simulation of perovskite solar cell with P3HT hole-transporting materials," *Nanophotonic*, vol. 11, no. 3, 2017.
- [54] Z. Zhang, X. Li, X. Xia, Z. Wang, Z. Huang, B. Lei and Y. Gao, "High-Quality $(\text{CH}_3\text{NH}_3)_3\text{Bi}_2\text{I}_9$ Film-Based Solar Cells: Pushing Efficiency up to 1.64%," *Physical Chemistry Letters*, pp. 3-10, 2017.
- [55] R. L. Z. Hoye, R. E. Brandt, A. Osherov, V. Stevanović, S. D. Stranks, M. W. B. Wilson, H. Kim, A. J. Akey, J. D. Perkins, R. C. Kurchin, J. R. Poindexter, E. N. Wang and Mou, "Methylammonium bismuth iodide as a lead-free, stable hybrid organic-inorganic solar absorber," *Chemistry*, vol. 80401, pp. 2605-2610, 2016.
- [56] "TEL nanotech museum," [Online].
- [57] "DoITPoMS," 2014-2018. [Online]. Available: https://www.doitpoms.ac.uk/tlplib/semiconductors/energy_band_intro.php. [Accessed 25 May 2019].
- [58] A. Kitai, Principles of solar cells, leds and diodes, West Sussex : john wiley and sons ltd, 2011.